UNIVERSITY OF NOVA GORICA
GRADUATE SCHOOL

COMPARISSON BETWEEN INDIUM TIN-OXIDE AND FLUORINE-DOPED TIN-OXIDE AS SUBSTRATES FOR ORGANIC LIGHT EMITTING DIODES

MASTER'S THESIS

Peter Krkoč

Mentor/s: prof. dr. Gvido Bratina

Nova Gorica, 2008

Acknowledgments

I was honored by the thrust shown to me by my mentor prof. dr. Gvido Bratina when he invited me to work in the field of organic semiconductors and thankful for his patience and foremost guidance from the very beginnings to the completion of this work.

I thank my coworkers: Alen Batagelj, Andraž Petrović, Dr. Egon Pavlica and Primož Rebernik Ribič for their immense amount of advice and explanations given with an even greater amount of patience. I am also thankful to all of the above mentioned people together with Mrs. Mavra Osirnik for the wonderful working atmosphere they created. Such a team makes returning to work every day a true pleasure.

There are various ways of help other than professional. For this type of help I thank my parents for the unconditional support troughout my studies and life. Without them this thesis wouldn't even have a foundation to grow from. Hvala!

A special thanks goes to Andreja for her moral support and understanding when work sometimes followed me out of the office.

Abstract

We have investigated the current-voltage characteristics and lifetime of organic light emitting diodes (OLED) with two different anode materials: indium tin-oxide and fluorine-doped tin-oxide. The rest of the OLED structure consisted of 8-hydroxyquinoline aluminum (Alq), N,N-diphenyl-N,N-bis(3-methylphenyl)- 1,1-biphenyl-4.4-diamine (TPD) and aluminum as the cathode material. Our results show that the current voltage characteristics depend strongly on the morphology of the anode. The absence of indium in fluorine-doped tin-oxide anode shows no superior performance in comparison to indium tin oxide. We believe this effect is overshadowed by the atmospheric influences on lifetime.

Keywords

organic semiconductors, organic light emitting diodes, lifetime, Alq, TPD, ITO, FTO.

Povzetek

Uvod

Organske sveteče diode (OSD) predstavljajo zanimivo alternativo anorganskim svetečim diodam, predvsem na področju zaslonov. Svojstvene lastnosti OSD omogočajo tudi povsem nove aplikacije, neizvedljive s katerokoli od obstoječih tehnologij. V mislih imamo predvsem aplikacije na področju razsvetljave in gibke zaslone. OSD lahko služijo kot vir svetlobe na veliki površini, npr. steni.

Raziskovanje OSD se začne v 50. letih 20. stoletja na kristalih antracena. Komercialna uporaba dobi zagon z uporabo več organskih plasti v 80. letih. OSD delimo na dve večji skupini in sicer polimerne OSD ter OSD na osnovi majhnih molekul. Tipičen predstavnik OSD na osnovi majhnih molekul je sestavljen iz plasti N,N-diphenil-N,N-bis(3-methilphenil)-1,1-biphenil-4.4-diamine (TPD), ki je prevoden v glavnem za vrzeli ter 8-hydroksikinolin aluminija (Alq), ki prevaja elektrone. S takšno konfiguracijo se ukvarjamo tudi v tem delu.

Kljub številnim prednostim in komercialno zanimivim lastnostim imajo OSD vsaj eno večjo pomanjkljivost - relativno kratko življensko dobo. Življenska doba varira z uporabljenimi materiali, obdelavo elektrod, načina izdelave ter načina enkapsulacije. Karakterizira se s polovičnim luminescenčnim življenjem, to je obdobjem v katerem pade svetilnost pri konstantni napetosti na polovico vrednosti nove naprave. Trenutno se maksimalne vrednosti gibljejo okoli 10000 ur. Degradacijo svetilnosti povzroča več procesov, ki potekajo na različnih časovnih skalah. Najbolj opazen način degradacije je rast temnih peg, ki zrastejo iz neemisivnih pik. V prisotnosti vode in kisika zavzemajo vedno večjo površino, dokler

temne pege ne prekrivajo celotne površine in dioda ne sveti več. Neemisivne pike so lahko posledica stikov med elektrodama. Stik lahko nastane zaradi hrapavosti katode ali senčenja (5. poglavje) na delčku nečistoče. Kaj povzroča rast temnih peg še ni povsem raziskano. Nekateri predlagajo spremembo strukture Alq molekule, medtem ko drugi predlagajo sproščanje kisika ter drugih plinov in s tem odstopanje katode od polprevodnika. Drug proces pri katerem opažamo manjšanje svetilnosti je prerazporeditev ionov pod vplivom zunanjega polja. Ioni nečistoč se porazdelijo tako, da nasprotujejo zunanjemu polju zaradi česar so tokovi in s tem luminescenca manjši. Podobno, preko zmanjšanja električnega polja, povzroča izgubo svetilnosti polnjenje pasti.

Proces, katerega smo poskušali zaznati preko vpliva na življensko dobo je bil difuzija indijevih ionov v organski polprevodnik. Za OSD se v veliki večini primerov kot substrat uporablja indij-kositrov-oksid (SnO_2:In_2O_3) oz. z angleško kratico ITO. Indij vsebovan v ITO-u difundira preko organskih plasti do katode. Za razliko od ITO-a kositrov oksid dopiran s fluorom (SnO_2:F) z angleško kratico FTO, ne vsebuje indija. S primerjanjem na ITO-u in FTO-ju temelječih diod, ki se med seboj razlikujeta le v vrsti anode, vsi drugi parametri pa so identični, smo želeli opazovati vpliv difuzije indija na življensko dobo.

Princip delovanja

Za opis delovanja svetečih diod obstajata vsaj dva pristopa. Prvi je transport po razširjenih elektronskih stanjih. Ta pristop je privzet iz anorganskih polprevodnikov, kjer imamo zaradi urejene kristalne strukture razširjena elektronska stanja po katerih se nosilci naboja gibljejo. Drugi je transport po lokaliziranih elektronskih stanjih, ki upošteva, da je prekrivanje elektrkonskih stanj v molekulskih kristalih majhno. Čeprav sta oba modela konceptualno različna, dajeta rezultate, ki jih je eksperimentalno pogosto težko razlikovati. Model transporta po razširjenih elektronskih stanjih, ki temelji na konceptu poljskega toka in difuzije za transport v polprevodniku, ter termične emisije in tuneliranja na kontaktih, je bil uspešno apliciran in je laže implementirati kot transport po lokaliziranih elektronskih stanjih. Zato smo pri razlagi meritev privzeli slednjega.

Ključni procesi, ki se tičejo OSD so: vbrizgavanje nabojev iz kovinskih elektrod v polprevodnik, procesi na mejah med polprevodniki, transport v polprevodniku, ujetje in pobeg nosilcev naboja iz pasti, rekombinacija elektronov in vrzeli ter emisija ekscitonov.

Različni načini vbrizgavanja so upoštevani: temična emisija, tuneliranje in ohmski kontakt. S termično emisijo označimo dogodek, ko ima nosilec naboja večjo energijo kot je energijska bariera na meji med kovino in polprevodnikom. Tuneliranje pride do izraza, ko je višina bariere veliko večja v primerjavi s k_bT, kjer je k_b Bolzmanova konstanta, T pa temperatura. V tem primeru ima le majhen delež nabojev zadostno energijo, da gre preko ovire. Pretežni del nosilcev, ki preči oviro

to naredi s tuneliranjem. Nasprotno, ko je ovira primerljiva s k_bT postane kovinska elektroda neusahljiv vir nosilcev naboja. Polprevodnik, jih zaradi majhne mobilnosti ne more tako hitro odvesti, kot jih je kovina sposobna dostaviti. Zaradi tega pride v polprevodniku do nabiranja nosilcev naboja, ki spremenijo električno polje, in s tem vplivajo na tok. Ponavadi je celoten vbrizgan tok sestavljen iz kombinacije zgoraj naštetih načinov.

Mejo med dvema organskima polprevodnika lahko obravnavamo na podoben način kot mejo med kovino in polprevodnikom.

Nosilci naboja se gibljejo skozi polprevodnik s poskakovanjem iz enega lokaliziranega stanja na naslednje. V povprečju potujejo v smeri polja, ki je sestavljeno iz zunanjega polja zaradi pritisnjene napetosti in polja presežnih nosilcev naboja, ki so v polprevodniku. Narava poskakovanja se kaže v majhni mobilnosti in njeni korenski odvisnosti od električnega polja. Del toka predstavlja tudi tok zaradi koncentracijskega gradienta, ki pa je ponavadi majhen v primerjavi s tokom zaradi polja in ga zanemarimo. Za opis dogajanja v polprevodniku uporabljamo tri enačbe, ki povezujejo električno polje, gostoto nosilcev in električni tok. To so transportna, Poissonova, ter kontinuitetna enačba.

Pasti lahko interpretiramo kot potencialne jame za nosilce naboja. Nastanejo kot posledica kemičnih nečistoč, defektov v kristalu ali površinskih stanj, in igrajo pomembno vlogo pri optičnih in električnih lastnostih OSD. Nosilec, ki je ujet v stanje pasti se čez nekaj časa sprosti ali se rekombinira z nosilcem nasprotnega predznaka. Stanja pasti imajo velik vpliv na transport. Čeprav ujeti nosilci ne prispevajo k transportu, njihov naboj prispeva k spremembi električnega polja in tako vpliva na transport. Po analogiji iz fizike anorganskih polprevodnikov vsako lokalizirano stanje pod spodnjo mejo prevodnega pasu imenujemo elektronska past. Podobno, vsako stanje nad valenčnim pasom imenujemo past za vrzeli. V organskih polprevodnikih, še posebej tistih z amorfno strukturo sta sta valenčni in prevodni pas ponavadi nadomeščena z HOMO (ang. highest occupied molecular orbital) in LUMO (ang. lowest unoccupied molecular orbital) nivoji. Porazdelitev stanj je opisana z eksponentno, Gaussovo ali porazdelitvijo, ki je kombinacija obeh. Ker nimamo več ostrih robov valenčnega in prevodnega pasu, temveč zvezno porazdelitev nastane težava kako ločiti med transportnimi stanji in stanji pasti. Kot meja med temi dvemi stanji je postavljena transportna energija in je definirana kot energija v katero je najbolj verjeten preskok ne glede na začeno energijo nosilca.

Da OSD sveti mora priti do rekombinacije vrzeli in elektrona. To se ne zgodi direkno, ampak preko vmesnega stanja v katerem vrzel in elektron bivata nekaj časa skupaj. Temu stanju pravimo ekscitonsko stanje ali eksciton. Ekscitonov je lahko več vrst, delimo po tem kako blizu sta vrzel in elektron. Za primer kratkih razdalj, ko sta elektron in vzel oddaljena nekaj Å, ekscitonu rečemo Frenkelov eksciton. Wannier-Mottov eksciton pravimo stanju, ko sta vrzel in elektron na razdalji več 10 do 100Å. Za organske polprevodnike z neurejeno strukturo velja, da imamo

zaradi majhnih interakcij med molekulami predvsem prve, Frenkelove ekscitone. Rekombinacija ekscitona poteka na več načinov. Do nje lahko pride na lokaliziranih stanjih, defektih ali ker prideta dovolj blizu skupaj, da se rekombinirata zaradi Coulumbove interakcije. Vsaka rekombinacija ne prinese generacije fotona. Za vsako rekombinacijo imamo le 0.25 verjetnost, da bo stanje singletno. 75 % delež ekscitonov je tripletnih. Deaktivirajo se neradiacijsko. Tudi sigletno stanje se lahko deaktivira termično, zato je delež fotonov še manjši. Ko je rezultat rekombinacije foton se lahko ta ponovno absorbira ali pa ga zunaj zaznamo kot vidno svetlobo.

Eksperimentalne metode

Za proučevanje rasti organskih polprevodnikov smo uporabljali Veeco CP-II mikroskop na atomsko silo in sicer v dveh načinih delovanja: brezkontaktnem in prevodnem načinu. V brezkontaktnem načinu tipalo ne pride v stik z vzorcem in ga tako ne poškoduje. Ta metoda je uporabna za merjenje mehkih ali slabo obstojnih vzorcev. Tipalo je od površine vzorca oddaljeno 5 do 15 nm in nanj deluje privlačna van der Waalsova sila. V prevodnem načinu se konica tipala dotika površine oz. je tako blizu vzorca, da se elektronska oblaka okoli atomov tipala in vzorca prekrivata in lahko dejansko dosežemo atomsko resolucijo. Na tipalo začne zaradi Paulijeve prepovedi delovati močna odbojna sila reda velikosti 10^{-7}N. Pri tem na tipalo in vzorec pritisnemo določeno napetost in merimo tok. Na ta način lahko točkovno merimo I-V karakteristiko.

I-V karakteristiko smo merili z Keithey 2400 multimetrom. Multimeter ima vgrajen napajalnik s katerim na elektrodi vzorca pritisnemo napetost in hkrati merimo tok. I-V karakteristika je izvedena v nekaj sekundah, da bi bi se izognili degradacijskim pojavom v času merjenja.

Spektralne meritve smo opravili tako, da smo med OSD in detektor postavili monokromator CVI Digikrom DK 240, s katerem smo izbirali želene valovne dolžine. Za detektor smo uporabili Hammamatsu H6600-04 fotopomnoževalko. Njen izhod smo meril z Keithley 2400 multimetrom priključenim na računalnik. Na ta način smo spekter med 450 in 700nm pomerili v nekaj sekundah.

Degradacijo svetilnosti smo prav tako merili s Keithley multimetrom v povezavi z računanikom. Zajemali smo s hitrostjo 3 meritev na sekundo pri konstantni napetosti 22V.

Eksperiment

Izdelali smo dve vrsti svetečih diod, identičnih v vsem razen v substratu. Oba substrata, ITO in FTO sta bila debela okoli 100nm, narejena s kemičnim postopkom nanašanja. Izdelava se je pričela z jedkanjem obeh, ITO in FTO substratov na steklu. Jedkali smo del anode, kjer je nad njo bil kontakt za napajanje katode. S tem smo preprečili kratek stik, ki bi zlahka nastal ob prevelikem pritisku na katodo. ITO smo jedkali z raztopino HF ($1HF{:}1H_2O_2{:}10H_2O$), FTO pa z cinkovim prahom in HCl. Po jedkanju smo substrate očistili v acetonu in izopropanolu. Najprej so se

5 minut namakali v vrelem acetonu, nato smo jih dali v ultrazvočno kopel, prav tako za 5 minut. Korak smo še enkrat ponovili z izopropanolom namesto acetona. Med vsako kopeljo so bili vzorci temeljito sprani z deionizirano vodo. Takoj po čiščenju smo vzorce posušili s curkom dušika in vstavili v nosilec z dvema maskama, ki sta omogočali naparevanje več plasti. Nosilec je bil vstavljen v vakuumsko komoro. Pri tlaku okrog 10^{-7}torr smo najprej naparili 125nm TPD-ja nato pa še 50nm Alq. Brez prekinitve tlaka smo zamenjali masko in naparili Al katodo na vzorce pri katerih smo merili I-V karakteristiko in svetilnost. Pri vzorcih kjer smo merili pokritost substrata z organskim polprevodnikom, Al katoda ni bila naparjena. Takoj po naparevanju so bili vzorci vzeti iz komore in pričeli smo z meritvami.

S takšno konfiguracijo plasti se je vedno dogajalo, da je svetil samo vzorec z ITO substratom, FTO vzorec pa ni svetil ali pa je svetil le za nekaj sekund, potem v trenutku popolnoma ugasnil. S pomočjo mikroskopa na atomsko silo, predvsem v prevodnem načinu smo ugotovili, da je FTO še vedno viden skozi plasti polprevodnikov in pride v direkten kontakt z katodo. Sklenili smo preučiti rast TPD na FTO z namenom, da odkrijemo pogoje pri katerem dosežemo popolno prekrivanje pri čimtanjši plasti. Majhna debelina je zaželena, saj omogoča nižje napetosti za dosego istega toka. TPD z debelino 125nm smo na FTO naparevali pri treh hitrostih: 1.4Å/s, 5.5Å/s in 8.7Å/s. Slika 4.7 prikazuje delež pokrite površine, merjenje z mikroskopom na atomsko silo v prevodnem načinu. Za mejo med pokritim in nepokritim delom smo izbrali mejni tok 1.3nA skozi tiplo mikroskopa. Iz meritev je razvidno, da hitrost naparevanja nima vpliva, ki smo ga želeli oziroma z nobeno hitrostjo nismo dosegli popolnega pokrivanja. Ker hitrost naparevanja ni dala želenih učinkov smo povečali debelino TPD-ja na 170nm. Debelina Alq in način priprave vzorcev so ostali isti. Prav tako pogoji naparevanja, pri čemer smo za TPD izbrali hitrost 9.6Å/s. S povečanjem debeline smo dosegli delovanje vzorcev s FTO substratom, kar je omogočilo meritve tokovno napetostnih karakteristik, spektroskopske meritve ter meritve življenske dobe.

Rezultati

Da bi razložili tokovno napetostne karakteristike smo uporabili naslednje predpostavke modela transporta po razširjenih elektronskih stanjih. Kontakte med kovino in polprevodnikom lahko obravnavamo kot ohmske s čemer lastnosti polprevodnika določajo tok. TPD ima dovolj veliko mobilnost vrzeli, da omogoča hiter transport od anode do TPD/Alq meje. Transport tako lahko obravnavamo kot enopolaren. Njegove karakteristike določa Alq plast, ki je v tem smislu ozko grlo naprave. Pretežen del padca napetosti se zgodi v plasti Alq v katerem so nosilci naboja elektroni. Rekombinacijska cona v Alq je majhna v primerjavi z debelino. Na mejah TPD/Alq ter Alq/Al predpostavljamo ohmske kontakte. S temi predpostavkami smo poskušali razložiti velike razlike med I-V karakteristikami obeh vzorcev. Tok skozi FTO vzorec je bil namreč dva velikostna reda večji kot tok

skozi ITO vzorec. Četudi sta povprečni debelini slojev enaki, zaradi odvisnoti toka od napetosti in debeline ne dobimo istega toka pri dani napetosti, ko seštejemo vse delne tokove pri različnih lokalnih debelinah Alq. Vpeljali smo efektivno debelino, to je debelino, ki da enak tok, kot je vsota delnih tokov na hrapavem vzorcu. Na tak način smo zračunali, da je efektivna debelina Alq na ITO vzorcu 48, na FTO pa le 11nm, pri isti povprečni debelini 50nm. Efektivna debelina v razmerju 1:5 lahko povzroči tokovne razlike v razmerju 1:200. Od 5V naprej vzorec prevaja v TCLC (Trap Charge Limited Current) režimu - to je reimu v katerem tok omejujejo zapolnjene pasti. Pod 5V je opazna tudi ohmska komponenta.

Kot že dokumentirano v literaturi so se tud pri naših vzorcih pojavile neponovljive anomalije pri I-V meritvah. To se pokaže tako, da ima I-V krivulja pri nekaterih napetostnih območjih področja negativne diferenčne upornosti. V tem režimu prevajanja, ne sveti celotna površina, temveč le lokalizirana področja. Spekter je na teh področjih širok in prezežno v infrardečem območju, zatorej verjetno ni posledica elektronskih prehodov v Alq. Iz tega sklepamo, da pretežni del toka teče skozi lokalizirane poti in ne uniformno preko celotnega vzorca. Ker se v našem delu zanimamo predvsem za homogen transport skozi organke plasti, smo se temu režimu poskušali izogniti.

Spektroskopske merive obeh vzorcev ne pokažejo opaznih razlik. To smo tudi pričakovali, saj je spekter odvisen le od elektroluminescenčnih lastnosti Alq. Če bi tudi EL potekala tudi v plasti TPD, bi pričakovali, da se bo cona rekombinacije pomikala s pritisnjeno napetostjo, kar pa se pri meritvah pri 10, 12, 14, 16 in 18V ni pokazalo.

Da bi bolje razumeli procese degradacije smo meritve normalizirali po času in intenziteti. Meritvam smo prilagodili funkcijo, ki vsebuje vsoto 3 eksponentnih funkcij z različnimi časovnimi konstantami. Pri obeh tipih vzorcev so bile konstante približno enake zato smo izločili vpliv difuzije indija na degradacijske procese.

Zaključki

Z mikroskopom na atomsko silo smo zaključili, da TPD in Alq rasteta v otokih. Popolno prekrivanje ni doseženo dokler ni presežena določena debelina. Debelina potrebna za popolno prekrivanje je zaradi hrapavosti substrata relativno velika v primerjavi z standardnimi debelinami OSD, dokumentiranimi v literaturi. Kar se tiče življenske dobe je malo verjetno, da je difuzija indija odgovorna za degradacijo svetilnosti na merjenih časovnih skalah. Življenske dobe več tisoč ur so bile namreč zabeležene na OSD na ITO substratih. Hitra degradacija je bila najverjetneje posledica morfoloških sprememb v organskih plasteh. V luči sedanjega znaja bi nekatere stvari zastavili drugače. Uporabili ravnejši FTO, po možnosti s podobno hrapavostjo kot ITO. Vzorce bi pred naparevanjem obdelali s plazmo, ki bi še dodatno zravnala površino. Površino bi z istim namenom prekrili s tanko, $\sim$10nm debelo plastjo bakrovega ptalocianina. Z enkapsulacijo ali meritvami v vakuumski

komori bi se lahko izognili vplivu kisika in vode ter na ta način morda podaljšali življensko dobo do te mere, da bi postali vidni vplivi indija.

Večja razlika kot pri življenski dobi je opazna pri tokovno napetostnih karakteristikah. Tokovi skozi vzorce na FTO substratu so dva velikostna reda večji kot tokovi skozi vzorce na ITO. To razliko pripisujemo veliki hrapavostjo FTO substrata.

Ključne besede

organski polprevodniki, organske sveteče diode, življenska doba, Alq, TPD, ITO, FTO.

Contents

Chapter 1 Introduction

1.1 Organic light emitting diodes

Organic semiconductors (OS) have a great potential to expand and in some areas replace the use of their inorganic counterparts. The replacement might occur in the area of low cost, low performance electronics (price tags, disposable cell phones), while flexible displays represent a totally novel application. One of the branches of the OS technology are organic light emitting diodes (OLEDs). Wether as pixels in organic displays or as general lighting devices, their indisputable advantages are bound to place them to use.

OLEDs are most commonly found in the form of one or more thin organic films sandwiched between two metal contacts. They have been investigated since the 1950s. The research begun on single crystals of anthracene and already at that time an operating organic electroluminescent display was developed showing one possible application of the developing technology. Unfortunately several drawbacks prevented mass use of the these early devices. Neither high enough light output nor sufficient stability could be achieved, namely because the crystal thickness was in the micrometer range, together with the difficulties in reproducing crystal growth and preparing stable and sufficiently well-injecting contacts.

In the 1970s considerably thinner (well bellow one micrometer) crystal films were prepared by vacuum vapor deposition or the Langmuir-Blodgett technique showing better performance than single crystal OLEDs. With lower thickness the same electric field as in the single crystal OLED type could be achieved at a considerably lower voltage. Besides the morphological instability of these polycrystalline films there was an additional problem of fabricating pinhole-free films from these materials. These problems were overcome in the early 1980s by the usage of morphologically stable amorphous films.

Another step forward towards better performance was achieved when several layers of different materials were used instead of just one. With these multi layer devices a better balance of the number of charge carriers of opposite sign was

achieved which further lowered the operating voltage by reducing the mismatch of energy levels between the organic materials and the electrodes. With this multiple-layer structure OLEDs found commercial use mainly in the form of flat panel displays for car radios, telephones and cameras [1].

OLEDs come in many varieties. The two main branches are molecular or small molecule OLEDs and polymer-based OLEDs, also called PLEDs. A typical molecular OLED consists of a thin layer of CuPc or polyaniline as a hole injection material and N,N'-diphenyl-N,N'-bis(3-methylphenyl)-1,1'-biphenyl-4.4'-diamine (TPD) or N,N -bis(l-naphthyl)-N,N -diphenyl-1,1 -biphenyl-4,4 -diamine (NPB) as hole transporters. The most widely used electron transport and emitting material is tris-8-hydroxyquinoline aluminum (Alq). It is popular due to it's morphological stability, easy purification and good emission properties [2]. Molecular OLEDs are usually deposited by vacuum evaporation while polymers are spin-coated or inject printed. Typical representatives of PLEDs are PEDOT/PSS as a hole transporter and MEH-PPV as the electron transporting and emitting layer [3]. Also hybrid OLED compositions exist combining the advantages of both OLEDs and PLEDS. As contacts, a transparent high work function material, usually Indium Tin Oxide (ITO), is used as the anode and a low work function material like Ca, Al or Mg:Ag and Li:F alloys as the cathode. Other criteria are also contact stability and non reactivity. Aluminum is frequently used for the non encapsulated OLEDs due to its moderate reactivity compared to Magnesium or Calcium [4]. Hybrid materials between metals and OS also exist. Alq can be for example doped with Li with the molecular ratio of unity. The benefits are a better conductivity and barrier lowering.

Despite many advantages, OLEDs have at least one weak point: relatively fast luminance degradation. OLED durability is characterized with its half life: the time in which its luminescence reaches one half of the value of a new device. Average lifetimes of OLEDs are about 10000 hours which is probably the main reason why the technology is not yet found in big-screen devices. A variety of processes contribute to OLED degradation on different timescales. Degradation in the form of growing nonemissive (black) spots was initially attributed to local heating caused by short circuits which led to cathode delamination. More recent studies revealed that the nonemissive spots have bubble-like structures filled with gasses (mostly oxygen). They presumably evolve in the course of electrochemical and photoelectrochemical processes in the presence of water [4]. Others [5] report that mechanisms involving replacement of the oxyquinoline moieties in the Alq complex with water are responsible for the degradation. Mobile ions and filling of traps have also been reported [2, 6, 7].

1.2 Motivation and scope

Since the high efficiency bilayer OLEDs [8] were introduced, these devices underwent a great development in terms of material choice and structure. In spite of this evolution, ITO continues to be the material of choice regardless its known limitations.

The chemical condition of the ITO electrode is affected by the particular ITO cleaning procedure which means that special care has to be taken when manufacturing efficient and reproducible devices. It has been shown that the work function of ITO can vary as much as ∼0.8eV for a HCL treated and HCL+UV ozone treated substrate. The variations between other cleaning procedures are also considerable [9]. The work function has an effect on the I-V characteristics and thus on turn-on voltage and light output. The turn-on voltage is the voltage at which the emission surface becomes visible to the human eye in the dark. But a higher work function does not necessarily imply a lower turn-on voltage since surface and interfacial chemistry is also important in determining charge injection [9, 10]. Another drawback using ITO is that Indium contaminates the organic layers. Indium originating from the ITO substrate in polymer OLED has been measured by XPS technique [11]. The contamination is observed immediately after fabrication, prior to device operation and may reduce the radiant recombination [12]. During device operation Indium contaminates the cathode. The main OLED degradation process is characterized by local distortions in the cathode surface which in term evolve into domelike structures which finally collapse leaving behind a volcano-like nonemissive area. It has been measured for small-molecule OLEDs, by means of scanning photoelectron microscopy, that after the collapse of the dome, ITO is exposed and In-containing species are deposited on the cathode [13]. For polymer OLED a similar phenomena has been observed.[14].

OLEDs with tin-oxide (TO) as the transparent electrode were demonstrated [12], but the lower work function and the higher electrical resistivity compared to ITO inhibited a wider use of TO in OLEDs.

For this reason we decited to use another material as the anode for OLEDs and explore what are its influences on light output and life time. Fluorine-doped tin-oxide (FTO) has a transparency and resistance similar to that of ITO and is not as cleaning procedure dependant as ITO. It is also much more stable from the chemical point of view. It has a lower work function than ITO but intermediate layers such as PEDOT:PSS can be used to effectively reduce the potential barrier for positive charge carriers [15]. In light of these facts we have decided to try FTO as a substrate for our small-molecule OLEDs.

1.3 Text structure

This text is structured as follows. After the introduction a brief overview of OLED operation is given in chapter 2. Chapter 3 explains the experimental part of the work: sample preparation and measurement techniques. Chapter 4 deals with TPD growth on FTO substrate and the difficulties encountered while trying to achieve full coverage of the substrate which is essential for successful OLED operation. Chapter 5 compares the measurements made with the two substrates and chapter 6 summarizes the conclusions.

Chapter 2 Operation of organic light emitting devices

2.1 Operation model

2.1.1 Introduction

It must be stated that at least two different approaches exist that try to explain and model the operation of OLEDs: the continuum and the hopping approach [17]. The continuum model is inherited from the field of inorganic semiconductors. It assumes a periodic potential formed by the crystal lattice that creates extended states called bands [18]. Charge carriers that occupy these states are allowed to move nearly as free, with a different effective mass. But organic semiconductors, especially amorphous ones do not posess a degree of order high enough for the onset of electronic energy bands. Instead, states are localized. Usually a Gaussian like energy distribution around the molecular highest occupied molecular orbital (HOMO) and lowest unoccupied molecular orbital (LUMO) states is considered. A carrier sitting at a particular state has a certain probability to hop to a neighboring state under the influence of an applied field. Monte Carlo simulations are usually employed to model this kind of transport. Although these two models are conceptually very different they both yield predictions that are experimentally often hard to distinguish. In this writing we adopted the continuum model. Continuum band models based on the concepts of drift and diffusion for bulk transport and thermionic emission and tunneling at contacts have been successfully applied to OLEDs and are simpler to implement.

The key phenomena concerning OLEDs is electroluminescence, a phenomena where light is generated from condensed matter by electrical excitation other than black-body emission. In order to understand and control (enhance) electroluminescence several other physical processes underlying the operation of OLEDs have to be understood. These processes are: charge injection from metallic electrodes into the organic layers, OS-OS interfaces, charge transport, trapping and detrapping,

electron-hole recombination and exciton emission.

2.1.2 Charge injection

Charge carriers that undergo radiative recombination have to be supplied to the emitting media trough contacts. When an organic semiconductor (OS) makes contact with a metal, their Fermi levels align. The barrier height for electrons ϕ_{bn} and holes ϕ_{bp} can be expressed as:

$$q\phi_{bn} = q(\phi_m - \chi)$$
$$q\phi_{bp} = E_g - q\psi_{bn} \tag{2.1}$$

where q is the unit charge, $q\phi_m$ the metal work function, χ the electron affinity for the semiconductor and E_g the semiconductors bandgap. Under bias there is an additional barrier lowering due to the added effect of the applied field and the image force [19].

The calculation of the barrier reduction assumes that the charge of an electron in the semiconductor close to the metal-semiconductor interface attracts an opposite surface charge in the metal which exactly balances the electron's charge so that the electric field surrounding the electron in the semiconductor does not penetrate beyond the surface and into the metal. The electric field in the semiconductor is identical to that of the carrier itself and another carrier with opposite charge at equal distance but on the opposite side of the interface. The charge experiences the force of the image charge in the metal and the applied electric field F. The potential energy of the charge at a position x from the electrode therefore is:

$$U = \frac{q^2}{4\pi\epsilon\epsilon_0 x} + qFx \tag{2.2}$$

where F is the applied electric field and ϵ_0 the permittivity of free space. The magnitude of the lowering is given by the condition that $\frac{dU}{dx} = 0$. The derivative has its minimum x_{min} at $\sqrt{q/16\pi\epsilon\epsilon_0 F}$. By inserting x_{min} into equation 2.2 we find that the barrier height is reduced by (Figure 2.1):

$$\Delta\Psi = \sqrt{\frac{qF}{4\pi\epsilon\epsilon_0}}$$

OS have a much lower permittivity than inorganic semiconductors (IS). For example typical values for OSs are $\epsilon \approx 3$, while silicon for example has $\epsilon = 12$. This increases the importance of image force barrier lowering compared to IS.

The barrier heights are of importance because they affect the current density: the lower the height the more carriers will have enough energy to overcome it. Several types of injecting contacts have been proposed for device models:

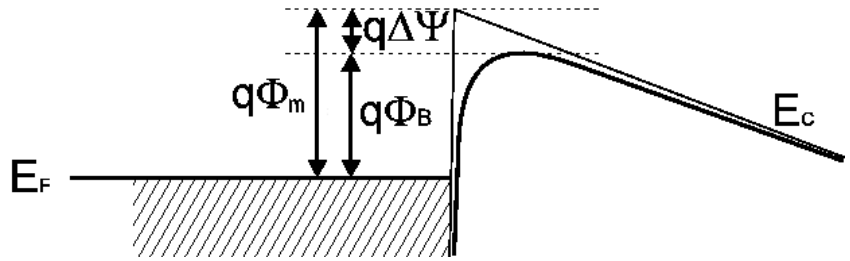

Figure 2.1: Energy band diagram for the interface between a metal and a semiconductor. The metal work function is $q\psi_m$. The potential energy due the applied field and the field by the image charge varies as U=$\frac{q^2}{4\pi\epsilon\epsilon_0 x} + qFx$ Since the barrier is lowest at the condition $\frac{dU}{dx} = 0$, the minimum occurs at $x_{min} = \sqrt{q/16\pi\epsilon\epsilon_0 F}$. The barrier is lowered by $q\Delta\Psi = \sqrt{\frac{qF}{4\pi\epsilon\epsilon_0}}$. E_F and E_C denote the metal Fermi level and semiconductor conduction band-edge respectively

1. **Thermionic emission**

   Thermionic emission occurs when charge carriers have energies greater than the barrier height. The Richardson-Schottky (RS) equation is used to account for thermionic emission current:

   $$J_{RS} = A^* T^2 exp\left(-\frac{\phi_b - \beta_{RS}\sqrt{F}}{k_B T}\right) \tag{2.3}$$

   with the Richardson constant $A^* = 4\pi q m_0 k_B^2/h^3$, $\beta_{RS} = \sqrt{q^3/4\pi q\epsilon\epsilon_0}$, ϕ_b is the zero-field injection barrier height for electrons or holes, m_0 is the free electron mass, k_b the Boltzmann constant, ϵ the relative dielectric constant and T the absolute temperature.

2. **Tunneling**

   Tunneling becomes the prevalent form of injection, when the barrier is high in comparison to $k_b T$ and few carriers have energies exceeding it. Instead carriers tunnel trough the barrier. The Fowler-Nordheim formalism is often used:

   $$J_{tun} = \left(\frac{3q^2F^2}{8\pi h\phi_b}\right) exp\left(-\frac{8\pi\sqrt{2qm^*\phi_b n^3}}{3hF}\right) \tag{2.4}$$

   with h being the Planck constant. The equation is valid for electrons (J_{ntun}) and holes $J_{ptun}$with the appropriate barriers ϕ_b and effective masses m^*.

3. **Ohmic contacts** A contact is considered to be ohmic when the metal electrode acts as an inexhaustible carrier source. In this case the metal-organic contact injects more carriers than the bulk OS has in thermal equilibrium [1], leading to the alternation of the electric field at the injecting contact which in turn obstructs further injection. This regime of operation is called space charge limited injection (SCSL). Ohmic contacts are often adopted for devices with low barriers $\phi_b < 0.3eV$.

Not always only one type of injection prevails for all regimes of device operation. Thus a model has been proposed [20] in which three current components are accounted for. The total injected current density is written as a sum of thermionic and tunneling components in addition to a back flow recombination current. The thermionic current density at the contacts is written in terms of effective recombination velocities so the total current density for electrons and holes is given by:

$$J_n = -qv_n(n - n_e) + J_{ntun} \qquad J_p = -qv_p(p - p_e) + J_{ptun} \tag{2.5}$$

where v_n and v_p are the recombination velocities for electrons and holes, respectively, n_e and p_e their equilibrium carrier densities at the contacts and n and p the hole densities at the interface. For OS the recombination velocities take the form of [16].

$$v_n = \frac{16\pi(k_BT)^2\mu_n}{q^3} \qquad v_p = \frac{16\pi(k_BT)^2\mu_p}{q^3} \tag{2.6}$$

The backflow contributions qv_nn_e and qv_pp_e in equation 2.5 and the values v_n and v_p are obtained by following reasoning. A charge carrier, say, electron will on average recombine with a hole if it comes within r_c of the hole. At r_c its potential energy $U = e^2/4\pi\epsilon\epsilon_0 r_c$ equals kT. r_c is known as the Coulomb radius.

$$r_c = \frac{e^2}{4\pi\epsilon\epsilon_0 kT}$$

At $x_c = r_c/2$ from the metal-semiconductor interface the recombination current for electrons from the semiconductor to the metal will be:

$$J_{rec} = n_eq\mu_nF(x_c) = 16\pi\epsilon\epsilon_0(kT)^2n_e\mu_n/e^2.$$

v_n is defined as $v_n = J_{rec}/n_eq = 16\pi\epsilon\epsilon_0(kT)^2n_e\mu/q^3$. v_p is defined similarly for holes.

2.1.3 OS-OS interfaces

Single layer OLEDs tend to be inefficient due to the imbalance of carriers of the opposite sign since it is hard to find contacts with work functions that will make equal barriers with the OS for electrons and holes [17]. The anode material is also restricted to ITO or other transparent material eg. semiconducting oxides of tin, indium, zinc, and cadmium and metals such as silver, gold, and titanium nitride. Furthermore OS tend to have mobilities for holes several orders of magnitude different than for electrons meaning that the density of the slower charge carriers will be largest next to it's injecting electrode while the faster carriers will be more evenly distributed. Consequently, the recombination will predominately occur next to the slower-carrier injecting electrode leading to exciton quenching, a phenomena where excitons de-excite nonradiatevely at the metal-OS interface. The imbalance is normally so great that despite the accumulation of the slower, and usually minority charge carriers the majority carriers will pass the device without recombining, resulting in a low quantum yield. The situation is considerably improved by employing a bilayer structure. The problem of imbalanced injection and charge carrier transport is solved by choosing appropriate contacts for the hole and electron transporting materials so that they have similar barrier heights for both carrier types. The HOMO and LUMO levels of the hole and electron transporting layer (HTL and ETL, respectively) usually differ, and a barrier for the two types of carriers is formed at the OS-OS interface, causing charge buildup and further recombination improvement.

If there is no chemical reaction between the layers, the HOMO and LUMO band edges remain flat and the barriers at the interface for holes and electrons correspond to the difference in band edge levels. A chemical reaction between the two materials causes the formation of additional states and band bending.

Different approaches have been taken in device modeling. One approach that provided good results is based on the assumption that the quasi-Fermi level must be continuous throughout the device (Figure 2.2). The quasi-Fermi level is the level where the state occupancy probability equals $\frac{1}{2}$ for nonequilibrium conditions ie. operation under bias. It can be used when time scales of interest are much larger than the time the particle needs to reach thermal equilibrium with the lattice. When the excess carrier concentration is small compared to the equilibrium carrier concentration, the quasi-Fermi level must be very close to the Fermi level.

Another approach is to treat the abrupt interface as a junction and apply a thermionic emission current coupled to the drift-diffusion process.

2.1.4 Charge transport

After carriers are injected into the OS, they are transported towards the opposite electrode (Figure 2.3). The carriers are highly localized and move from site to site

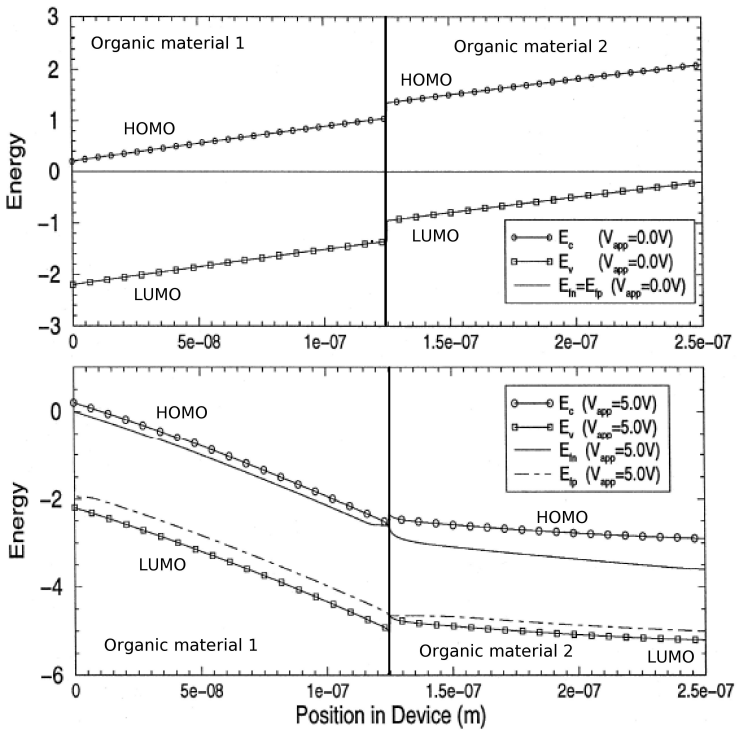

Figure 2.2: An OS-OS interface under equilibrium (top) and 5V forward bias (bottom). The box-marked lines denote the valence and circle marked lines the conduction band edges. The solid and chained lines denote the quasi-Fermi potential for electrons and holes, respectively [21].

by hopping. The mean free path is comparable to the molecule size. The hopping nature of the transport manifests itself in the low carrier mobility and its

$$\mu = \mu_0 exp(\sqrt{E/E_0}) \tag{2.7}$$

field dependence, where ν_0 is the zero field mobility and E_0 is the characteristic field. The electric field dependence of the mobility in equation 2.7 originates from an electric field induced barrier lowering of the coulombic barrier of the trap in the down-field direction. The phenomena is analogous to the image charge barrier lowering (Schotky effect) at the metal insulator interface.

The total current flow in an OS is determined by the electric field and the presence of carrier concentration gradients [22]. Since OLEDS have much greater lateral dimensions than the film thickness the equations governing the transport can be written in one dimensional form. For a bipolar device, that is a device with both holes and electrons as charge carriers the following equations define the model.

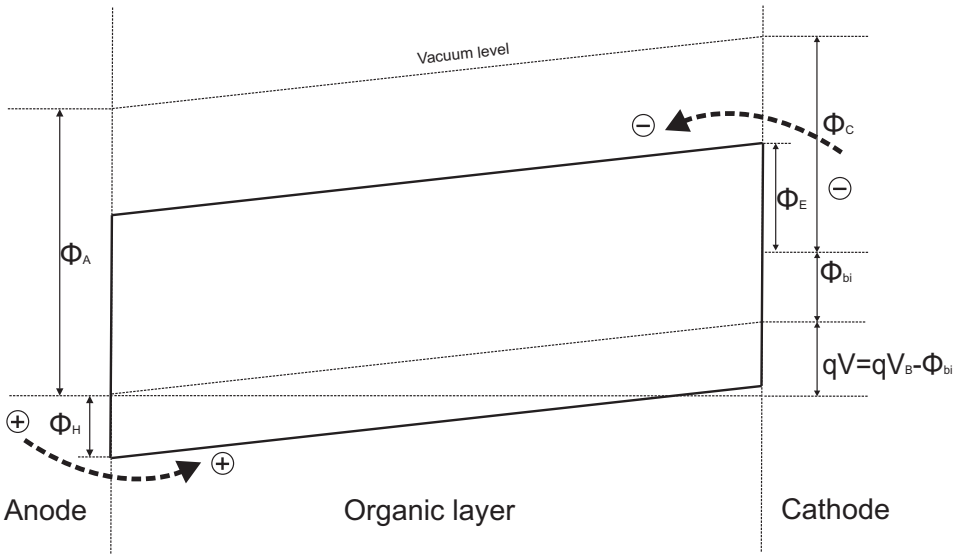

Figure 2.3: One layer OS sandwiched between two different electrodes under bias. The voltage drop occurs virtually entirely over the OS. Φ_A, Φ_C and Φ_{bi} denote the anode work function, cathode work function and the built-in potential, respectively. V denotes the applied voltage. The image force contribution to barrier lowering is omitted. Energy barriers Φ_E and Φ_H for electrons and holes, respectively are in first approximation given by the energetic offset between the work functions of the used metals and the energy levels of the organic material.

The drift diffusion equation for electron and hole current densities:

$$J_n = q\mu_n n(x)F(x) + qD_n\frac{dn(x)}{dx} \qquad J_p = q\mu_n p(x)F(x) + qD_p\frac{dp(x)}{dx} \tag{2.8}$$

The terms μ_n and μ_p denote the electron and hole mobility, respectively. D_n and D_p are the electron and hole carrier diffusion coefficients, respectively, related to its mobility by the Einstein equation: $D = \mu k_B T/q$ for either electrons or holes. $n(x)$ and $p(x)$ are the electron and hole densities, respectively. F is the applied electric field. The current is made up of two contributions: the current drifting due to the electric field plus the current due to the concentration differences. The diffusion term is often omitted since concentration gradients are normally small [17, 22, 1].

The Poisson equation: The solution of the Poisson equation yields the spatial

dependence of the electric potential:

$$\frac{dF(x)}{dx} = \frac{(n(x) - p(x) + N_d(x) + N_a(x))q}{\epsilon\epsilon_0} \tag{2.9}$$

where N_d and N_a are the ionized donor and acceptor impurity concentrations, respectively. $n(x)$ and $p(x)$ include charges contributing to the conduction and trapped charges.

The continuity equation

$$\frac{dn(x)}{dt} - \frac{1}{q}\frac{dJ_n(x)}{dx} = G - R; \qquad \frac{dp(x)}{dt} + \frac{1}{q}\frac{dJ_p(x)}{dx} = G - R \tag{2.10}$$

The terms $\frac{dn(x)}{dt}$ and $\frac{dp(x)}{dt}$ are zero in steady state operation. G and R denote the carrier generation and recombination rates discussed in section 2.1.6.

2.1.5 Trapping and detrapping

Traps may be interpreted as potential wells that trap carriers. They are caused by chemical impurities, crystal defects and surface states [22] and play an important role for optical and electric properties of OS based OLEDs.

Trapped charges may be released after a period of time or may recombine with carriers of opposite sign. In case the release rate is higher than the recombination rate the state is called a trap. If the recombination rate is higher the state is called a recombination center. Traps affect strongly the charge transport properties. Although trapped charges do not contribute to charge transport their coulombic charge will influence the electric field distribution in a device and therewith charge transport. In terms of classic semiconductor physics each localized state below the conduction band edge, which is able to capture an electron is called an electron trap. Similarly each state above the valence band able to capture a hole is called a hole trap. The density of states in OS, especially amorphous layers where the conduction and valence band are usually replaced by the LUMO and the HOMO levels, is better represented by a Gaussian-like distribution. In this case it is not obvious how to distinguish between a transport and a trap state. Further more both trap and transport states are localized. Figure 2.8a shows the transport states represented by a Gaussian-like distribution which gradually assumes an exponential form at it's edge 2.8b. A purely Gausian, purely exponential distribution (Figure 2.4) or multiple Gausian with more than one maximum is also used . The quantity E_t called transport energy takes the role of the energy delimiting transport and trap states. It is the energy that the trap states are most probable to be released to regardless of its initial energy. Each state below the transport energy is a trap while states above the transport energy are regular transport states.

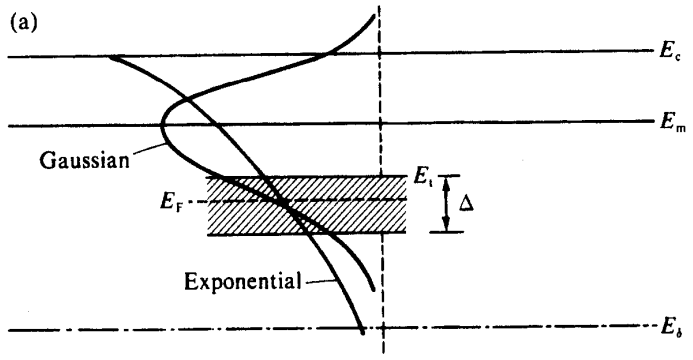

Figure 2.4: Comparison of Gaussian and exponential electron trap distributions. E_C is the conduction bandedge, E_F is the quasi-Fermi level and Δ the maximum energy interval sampled by the quasi-Fermi level in the course of normal operation [22]. E_t is the transport energy which delimits transport and trap states. It is the energy that the trap states are most probable to be released to regardless of its initial energy.

Deep traps near the center of the bandgap act either as non-radiative recombination sites or limit the effective carrier mobility. Measurements with thermally stimulated current techniques showed a broad distribution of traps in the range between 0.06 and 0.55eV for Alq and an isolated trap level at 0.12eV followed by a distribution of traps between 0.25 and 0.54eV for TPD [38]. In thermal stimulated current technique, the trapped charge carriers are released by heating up the sample with a linear temperature ramp, while the stimulated current is recorded as function of temperature. This directly yields the required activation energies for the charge transport independent of any selection rules. However, if one wants to relate the obtained activation energies to the energy position of the trap state, one has to take into account that both the thermal release of trapped charge carriers as well as the temperature dependence of the mobility which determines the recorded current. Usually, the temperature dependence of the mobility is neglected.

Traps situated on chemical impurities

An impurity molecule has in general a different ionization energy (the energy needed to remove an electron from a neutral molecule) and electron affinity (the energy required to detach an electron from a singly-charged anion) than the host material causing the basis for the formation of carrier traps. If the ionization energy of the impurity molecule is lower than of the host, the impurity site will behave as

a hole trap. In contrast, if the electron affinity of the impurity exceeds that of the host, the impurity will act as an electron trap. It can also act as a trap for both carrier types although the depth will differ for each of them [22].

Traps situated at crystal deformation

Crystal deformations cause local changes in the polarizability of the lattice. In turn this causes potential wells in which charge carriers are trapped. TPD and Alq do not form a crystal structure on ITO surface [1, 23, 35] but is found to be amorphous. Weather a solid has a crystalline or amorphous structure affects the mobility and mobility temperature dependence. A molecular crystal can have the mobility of $\mu > 1$ cm^2 V^{-1} s^{-1} and its temperature dependence goes as $\mu \propto T^{-n}$, $n > 1$. A strongly localized carrier e.g. amorphous media has the mobility $\mu \ll 1$ cm^2 V^{-1} s^{-1} with temperature dependence $\mu \propto exp(-E/kT)$ where E is an activation energy [24].

Traps at the surface

Two types of traps can exist on the surface and can be classified as being either intrinsic or extrinsic [22]. The intrinsic type of traps exist already on a atomically clean surface. For instance, the termination of a covalently bound crystal creates dangling bonds that can lead to localized states at the surface with trap energies in the crystal energy gap. In a molecular crystal there are no dangling bonds at the termination of a molecular crystal.

Extrinsic type of traps occur on contaminated surfaces. A metallic layer on an organic crystal for instance causes a region of high polarizability whereas the metallic orbitals can interact with the conduction levels of the OS to produce splitting of levels. 2.5

Traps are even more likely to occur at the surface since is it much more exposed to chemical impurities than the bulk material. Sample preparation must thus be done with great care to keep the surfaces as clean as possible.

It is argued that shallow traps need not to be explicitly introduced because they are included in the Poole-Frenkel mobility. Deep traps require an extra recombination term and inclusion in the Poisson equation. Because of its simplicity and good results an exponential decay of from the band edge to the bandgap is often assumed:

$$h(E) = \frac{H}{k_B T_C} \exp\left(-\frac{E}{k_B T_c}\right)$$

where H is the total trap concentration and T_c the characteristic temperature. By integrating the product of the trap density and the Fermi-Dirac probability function the trap concentrations for electrons n_t and holes p_t can be calculated:

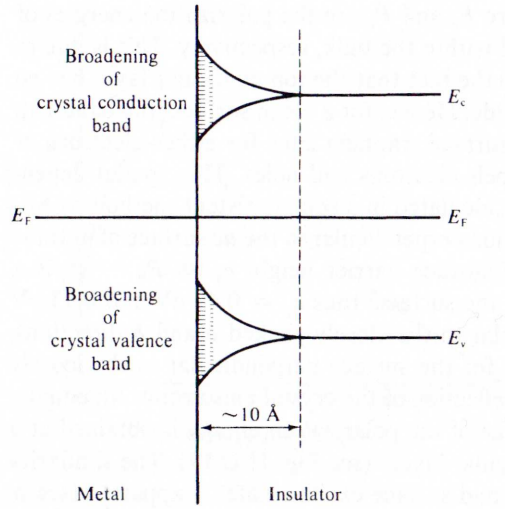

Figure 2.5: Splitting of states at the metal-OS interface. In the vicinity of the interface the valence and conduction band-edge of the OS is split due to the interaction of metallic orbitals.

$$n_t = H_n \exp\left(\frac{qU + E_{nq} - E_L}{k_B T_{cn}}\right) \qquad p_t = H_p \exp\left(\frac{E_H - qU - E_{pq}}{k_B T_{cp}}\right) \tag{2.11}$$

with H_n and H_p being the total corresponding trap concentrations, U is the potential measured from the band edge, E_L and E_H denote the LUMO and HOMO levels, respectively. T_{cn} and T_{cp} are the corresponding characteristic temperatures and E_{nq} and E_{pq} the quasi-Fermi levels. The subscripts n and p label quantities for electrons and holes respectively.

2.1.6 Carrier recombination and exciton emission

Carrier recombination

Electron-hole recombination involves the formation of excitons. Excitons are bound electron-hole pairs which can be classified according to the distance between the electron and the hole.

When the distance between the electron and the hole is more than an order of magnitude larger than the intermolecular separation $\sim 40 - 100\mathring{A}$ the exciton is called a Wannier-Mott exciton. They are most common in inorganic systems, where the interaction energy is great and electric constant is high in comparison to organic systems.

On the other extreme we have the Frenkel exciton which has a small radius ($\sim 5\mathring{A}$) in comparison to the separation between molecules. The electron from the small radius Frenkel exciton can be promoted to a nearest or next-nearest neighboring molecular site, but still remaining correlated with the hole. This type of excitons lie in between the other two extremes and are referred to as charge-transfer (CT) excitons. CT states can be either trapped or mobile. In the latter case the correlated electron-hole pair moves from lattice site to lattice site and is said to be delocalized. The three types of excitons are presented in figure 2.6

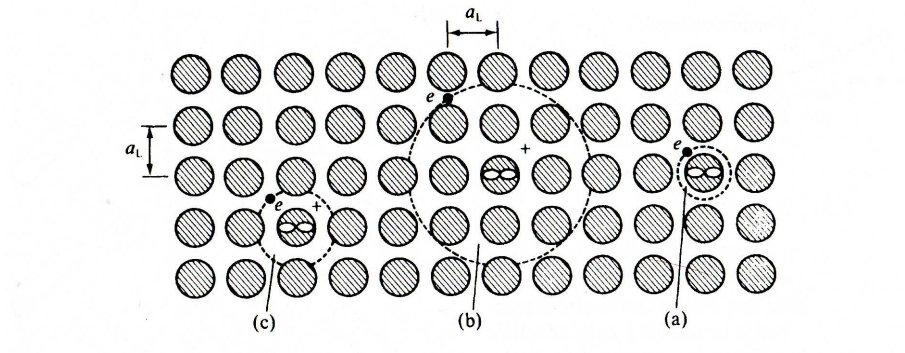

Figure 2.6: A schematic view of exciton types: Frenkel exciton with a small ($\sim 5\mathring{A}$) radius in comparison to molecular separation (a), Wannier-Mott exciton with an electron-hole radius of $\sim 40 - 100\mathring{A}$ (b) and an intermediate charge-transfer state. a_l is the lattice constant.

Excitons can recombine either radiatively or nonradiatively (Figure 2.7). When the decay involves generation of photons together with phonons the decay is said to be radiative. If the decay involves only phonons the exciton is said to decay nonradiatively. The routes of decay are the following [22]:

- Auger recombination - in the presence of localized states. The process involves three particles. First a charge (electron or hole) is trapped at a defect and a counter charge recombines with it forming a trapped CT state. In case another electron collides with the trapped CT state the recombination energy is used to impart kinetic energy to the colliding electron. In the vicinity of surface photoemission can occur.

- Auger recombination - band to band. Charge carriers recombine directly without forming intermediate exciton states. Their excess energy is given to another electron that can ionize.

- Recombination at defects. The decay occurs radiatively or nonradiatively at an impurity or imperfection. This type of recombination occurs at traps

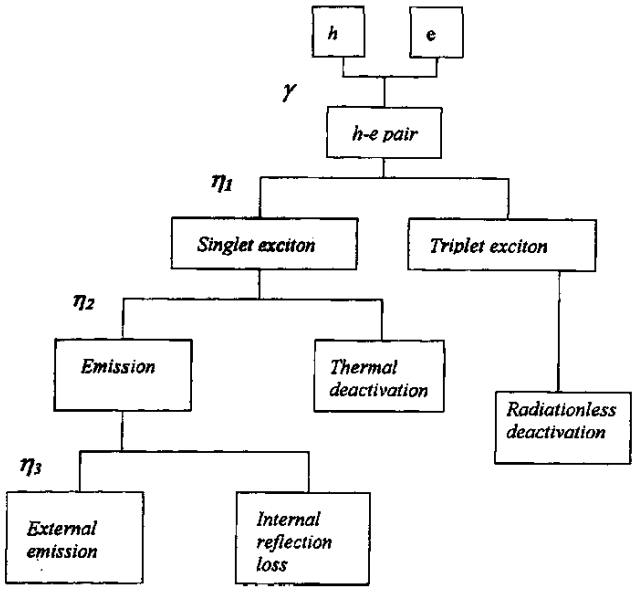

Figure 2.7: After formation excitons undergo different decay routes. If electron spins are arranged to form a triplet exciton the exciton undergoes a non-radiative recombination. If the exciton state is singlet it can deactivate thermally or emit a photon, which may or may not exit the device.

sites and is treated with the Shockley-Read-Hall model [25]. The resulting recombination rate R_{SRH} is:

$$R_{RSH} = \frac{np - n_i^2}{\tau_{p0}(n + N_C \exp -\frac{E_C - E_T}{k_B T}) + \tau_{n0}(p + N_V \exp -\frac{E_T - E_V}{k_B T})} \tag{2.12}$$

- Recombination with multi phonon emission. This is a process where trapped or free excitons decay nonradiatively.

- Recombination energy loss by cascade. This process involves two opposite charge carriers that come in within the Coulombic capture radius r_c defined as the distance at witch the particle kinetic energy is equal to the Coulombic attractive potential energy. In the absence of an external electric field the probability of recombination is $f(r) = 1 - \exp(-\frac{r_c}{r})$. In within the Coulombic radius, if the carriers loose energy by phonon emission, the probability of recombination increases exponentially.

- Langevin Recombination. If oppositely charged carriers are taken to be independent of each other and the mean free path of carriers λ is less than the capture radius $r_c = \frac{q^2}{4\pi\epsilon\epsilon_0 k_B T} \approx 1.710^{-6} cm$ the bimolecular recombination rate

can be calculated. The recombination of a charge pair can be described as two opposite charges drifting together under electrostatic mutual attraction. For computational simplicity we hold one charge, say hole, stationary. The electron has then the apparent mobility $\mu_T = \mu_e + \mu_h$. The current density of electrons attracted by the hole's field F at r_c is thus:

$$J = n_h q v_e = n_h q \mu_T F = n_h q \mu_T \frac{q}{4\pi\epsilon\epsilon_0 r_c^2}$$

yielding the total current I trough a sphere with radius r_c centered at the hole:

$$I = n_h \mu_T \frac{q^2}{\epsilon\epsilon_0}$$

The recombination rate equals the current: $\gamma n_h q = n_h \mu_T \frac{q^2}{\epsilon\epsilon_0}$. γ - called the bimolecular rate constant is thus: $\gamma = q\frac{\mu_e+\mu_h}{\epsilon\epsilon_0}$

For Langevin recombination to hold, another condition must be met. The free path λ of carriers must be shorter than the radius of capture. This condition is met in OS as the mean free path is of the order of the lattice parameter. The Langevin recombination rate R_L is then

$$R_L = np\gamma \tag{2.13}$$

The two dominant recombination mechanisms must be added to get the photon flux density:

$$\phi_{el} = \frac{k_r}{k_r + k_n} P_s (R_L + R_{SRH}) d$$

where k_r and kn are the radiative and nonradiative decay rates for an excited state, P_s is the probability that in a recombination event a singlet - radiative excited state will be created and d is the emissive layer thickness. The electroluminescent efficiency is defined as $\eta_q = \frac{q\phi_e l}{j}$, that is the ratio of emitted photons per unit area to the ratio of injected carriers. Another figure of merit concerning OLED is the energy conversion ration defined as: $\eta_p = \frac{E_e l}{P}$, where $E_e l$ is the power of the photon flux and $P = UI$ the power supplied to the device.

2.1.7 Summary

For a successful model all of the above processes must be consistent with each other. This means that in steady state operation the injected current must be equal at both contacts and throughout the device. Since current depends on the

electric field it is necessary to know its distribution throughout the device. Several contributions to the internal electric field in the device have to be considered. Firstly, there is the built-in field formed by the difference in the work functions of the anode and cathode. Secondly, there is the electric field due to the externally applied bias according to the dielectric constants of each layer. This two fields are uniform in each layer. Another two contributions are the space-charge and trapped-charge contributions to the electric field which arises from distributions of electrons and holes, within the device according to Poisson's equation. In order to get relevant results many material parameters must be known: density of states, barrier heights, field dependent mobilities, trap distributions, to name a few. Unfortunately unlikely inorganic semiconductors (IS) many of these parameters are often poorly characterized. To obtain these parameters independent measurements in preferably single layer samples have to be done. Mobility for instance is measured by time of flight techniques where carriers are generated at one electrode and transit time to the other electrode is recorded. Another way is to measure the time-resolved electroluminescent (EL) response, where one measures the time delay between the onset of a pulse voltage at the contacts and the appearance of EL [1]. In the case that position where EL occurs is known and one carrier mobility is much greater than other one gets: $\mu = d/tF$ where d is the device thickness and t the transit time. Ultraviolet photoelectron spectroscopy is usually used to determine work functions and HOMO and LUMO levels of OS and metals. Density of trap states and density of transport states can be measured by optically stimulated current (OST), thermally stimulated current (TSC) or thermally stimulated luminescence (TSL) [26]. In all of these three methods the states are filled, usually at low temperatures, to prevent a fast escape. The filling can be done either by photogeneration or electrical injection. In the next step, the carriers are released in a controlled way. In OSC the carriers are detrapped by interaction with incident light and the resulting current is measured as a function of wavelength. TSC measurements are done in similar way only that the detrapping energy is provided by heating up the sample with a linear temperature ramp. TSL is used for measuring trap depths of luminescent materials. Instead of measuring current the luminescence due to radiative recombination is measured. It is not obvious how to distinguish between a trap state and a regular transport state as charge transport in amorphous media is determined as hopping between localized states. Figure 2.8a shows the transport states usually represented by a Gaussian-like distribution gradually assumes an exponential form at it's edge 2.8b. The quantity E_t called transport energy takes the role of the energy delimiting transport and trap states. It is the energy that the trap states are most probable to be released to regardless of it's initial energy.

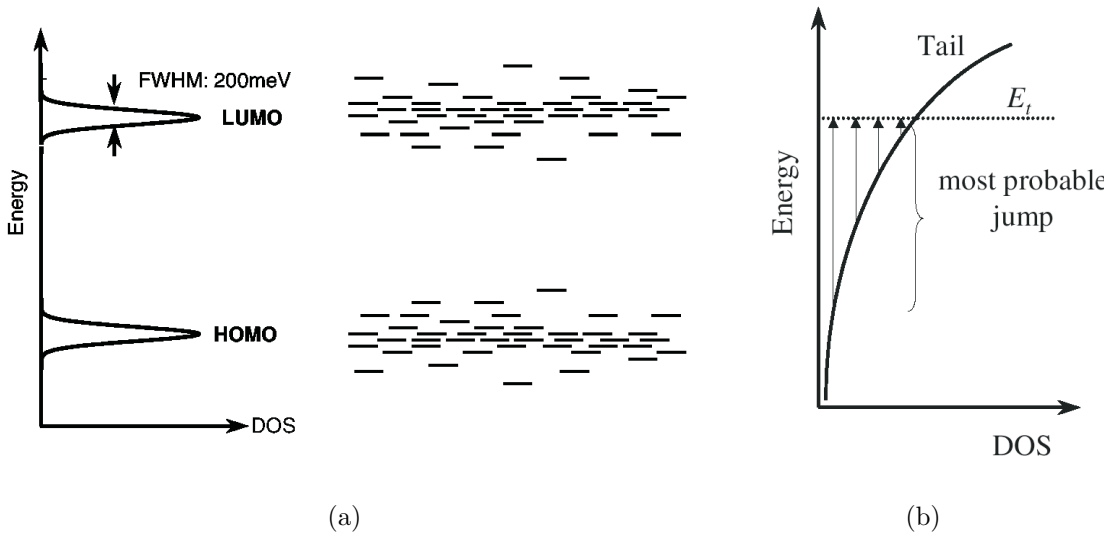

(a) (b)

Figure 2.8: (a) Gaussian energy distribution with an exponential tail in amorphous OS. The left part shows the density of states (DOS) dependence on energy. The right part shows a spatial distribution of states. (b) Exponential tail of carrier states. E_t is the most probable level the trapped carriers jump to and takes the role of the energy which delimits transport and trap states.

Chapter 3 Experimental methods

3.1 Sample preparation

ITO and FTO glass substrates form the basis from which our OLEDs were constructed. They consist of a few mm thick glass slab with an area of approximately 1cm^2. The glass has a thin film ∼100nm of ITO or FTO applied on one side by chemical vapor deposition technique [27].

Sample preparation can be divided in three steps: etching, cleaning and evaporation of the OS layers and electrode. The two types: ITO and FTO have undergone the same cleaning treatment and the same evaporation procedure. Etching was needed to avoid the two electrodes coming into direct contact. The cathode must not overlay completely the anode, otherwise a shorcircuit will almost unavoidably be made when making contacts. Figure 3.1a shows the arrangement of the layers and figure 3.1b the cross section. FTO was etched with Zinc in powder and 20% HCl while ITO was etched with HF solution (1HF:1H_2O_2:10H_2O).

After etching, the samples were cleaned. They were first immersed in boiling acetone for 5 minutes and subsequently ultrasonically cleaned in distilled water for the same amount of time. They were then boiled in 2-propanol and again ultrasonicated in distilled water. They were rinsed in deionized water after each ultrasonic cleaning. Immediately after cleaning, the samples were dried with nitrogen, mounted on the sample holder which was then mounted in the molecular beam epitaxy (MBE) chamber. In order to avoid deposition of dust particles on the clean surface, the loading aperture of the MBE chamber was located in the airflow of a flowbox. Once the samples were in the MBE chamber the OSs and the cathode were evaporated on top by molecular beam epitaxy technique. Both samples were evaporated simultaneously to ensure an equal film thickness, evaporation rate and pressure. Layer arrangement was accomplished by shadow masks placed in front of the sample. The masks were designed as a part of the sample holder. They would slide over and away from the sample by rotating a manipulator knob. After evaporation the samples were taken out of the chamber and tested in air.

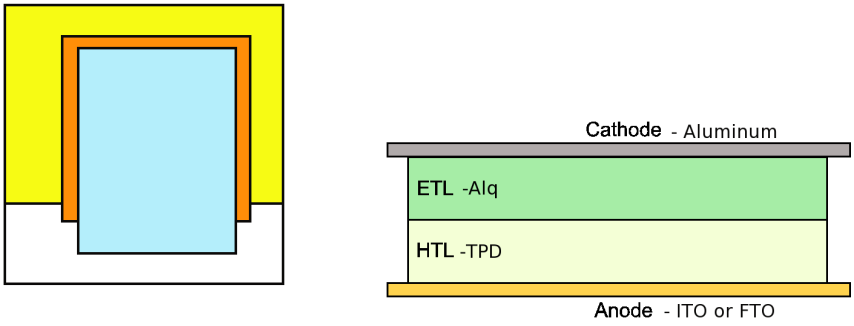

(a) (b)

Figure 3.1: (a) Top view of the sample showing the arrangement of layers. The biggest square is the whole sample. The yellow part is the non-etched ITO or FTO overlaid by organic materials (red) and aluminum electrode (blue), (b) a cross section of the OLEDs.

3.2 Molecular beam epitaxy

The backbone of an MBE setup consists of a ultra high vacuum (UHV) chamber, evaporation crucibles and the supporting measurement equipment. After the mounting of the samples into the chamber, organic material was evaporated with low temperature Knudsen effusion cells heated by electric current. The Knudsen effusion cells are depicted in figure 3.2.

A temperature controller was used in conjunction with a heater power supply in order to hold a constant temperature that conditions constant evaporation rate. The temperature variations were a few hundreds of a degree Celsius which results in negligible evaporation rate variations. Upon deposition of the organic layers the aluminum cathode was evaporated from a solenoid-shaped tungsten wire embracing an aluminum wire. The measurement of film thickness was done by a quartz thickness monitor (QTM). QTMs are based on the principle that the oscillating frequency of a quartz crystal is changed by the mass of a deposited film on its upper face. Measuring the change in oscilating frequency allows the determination of the thickness of a deposited film. Once the density of the evaporated material is entered into the system, the thickness is measured to a resolution of 0.1nm. Since the QTM was about 5cm away from the sample and the geometry of the effusion cells exhibit a strongly angle dependent flux the monitor reads a smaller thickness that the sample actually receives. Atomic force microscopy was thus used to calibrate the thickness monitor. Unknown thicknesses were deposited over only

Figure 3.2: Photograph of a low temperature Knudsen evaporation cell. The organic material and heating element are located within the stainless steel cylinder connected to the mounting element by thin metallic rods for low heat transfer.

half the sample area by using a shadow mask with a sharp edge, placed close to the same. The step between the area with no material and the area with the material deposited was thus short in order measure the step in one scan. From the measured height we could determine the tooling factor - the quotient between the flux at the sample and the flux at the quartz meter.

3.3 AFM microscopy

Since its invention in 1985 [28] the atomic force microscope (AFM) is one of the tools of choice when inspecting matter at the nanoscale. Our measurements were done with a Veeco CP-II Scanning Probe microscope shown in figure 3.3.

The building blocks of the AFM used are: a cantilever (probe) with a sharp tip, a laser and detector that detects the deflected light from the probe, a quartz translating stage and a feedback system that controls the translation (Figure 3.4). The probes are highly reflective in order to get a better signal on the detector. Their tip is sharp with a radius typically of about 10 nm. The piezoelectric tube on which the sample is mounted can translate in the plane of the sample (x-y direction) as well as perpendicular to the sample plane (z direction). The detector is an array of photodiodes and detects the position of the reflected laser beam. Scanning line by line in the x-y plane and recording the position of the tip, which follows the relief of the sample, gives us a 3 dimensional view of the topography. AFMs can operate in several modes, two of them used in this work are described in more detail.

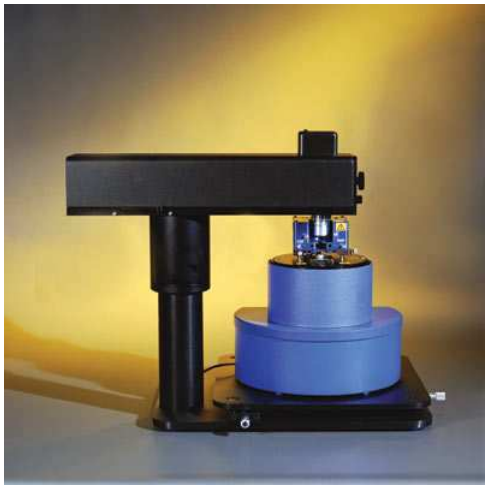

Figure 3.3: Veeco CP-II atomic force microscope. The sample is mounted on the top of the two blue cylinders. In the blue box above are the cantilever and laser. The black T shaped part contains the optics used to align the laser beam and cantilever.

3.3.1 Non contact mode

In this mode the probe vibrates 5-15 nm above the sample with a frequency close to its resonant frequency. As the probe moves across the sample the amplitude of the vibration, phase or frequency changes. The feedback loop varies the height above the sample in order to retain constant amplitude, phase or frequency (depending on the mode). The tip is never in direct contact with the sample which makes this mode less destructive in comparison to contact mode where the forces between the tip and sample are higher. This is particularly important for organic materials held together by weak Van der Waals forces.

3.3.2 Conductive mode

In conductive mode a current is measured trough the probe and sample. The probe must thus be made from a conductive material (Titanium-Platinum alloy for example). In all other aspects conductive mode is the same as contact mode. In contrast to non contact mode the tip of the probe is held in constant contact with the sample. As the probe moves across the sample the feedback loop tries to retain a constant repulsive force by heightening or lowering the sample. In this way we obtain the topography of the sample and the current at every point or the scanned array. The latter measurement was used to determine the coverage of organic material over rough fluorine doped tin oxide (FTO).

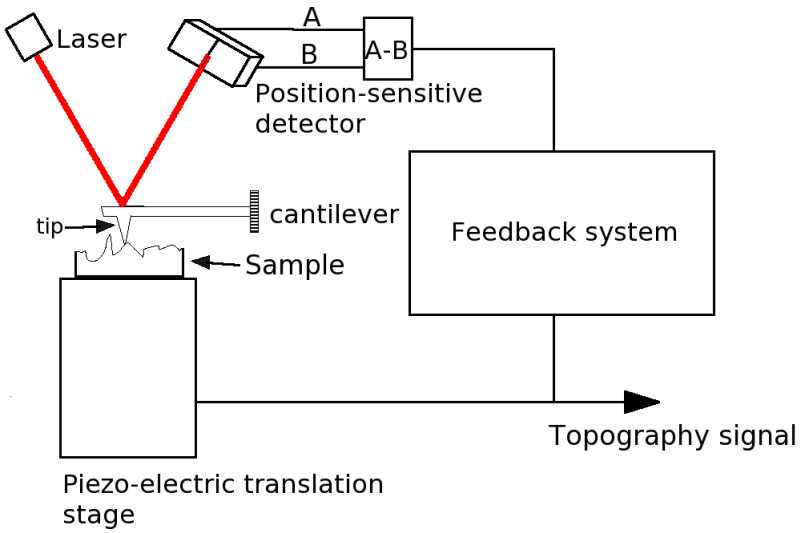

Figure 3.4: Scheme of AFM operation. A laser beam is reflected to a position-sensitive detector by a cantilever with a sharp tip probing the sample. For contact mode the cantilever scans the topography of the sample while the feedback system tries to maintain the reflected beam stationary by rising or lowering the sample. With an applied bias between the tip and sample we can obtain a current map of the sample. For non-contact mode the cantilever vibrates 5-15nm above the sample surface. As the cantilever scans over the surface the feedback system tries to maintain a constant amplitude.

3.4 Optical spectrum measurements

Spectrum measurement setup is schematically presented in figure 3.6. The computer driven CVI Digikroöm DK 240 monochromator allowed us to select a narrow part of the input light by means of rotating diffraction grating. The output intensity was measured with a Hammamatsu H6600-04 photomultiplier (PM). The PM response is shown in figure 3.5. PM's analog output was fed into a Keithley 2400 multi meter, connected to a personal computer. In such automated manner one spectrum sweep was completed in a matter of seconds. This is important, since we did not want luminescence degradation to affect the spectrum.

3.5 Current voltage measurements

Current-voltage measurements were made with a Keithley 2400 multi meter. It has a built-in power supply which enables us to bias the sample and measure the current all with one device. As before one I-V sweep was performed in a few seconds

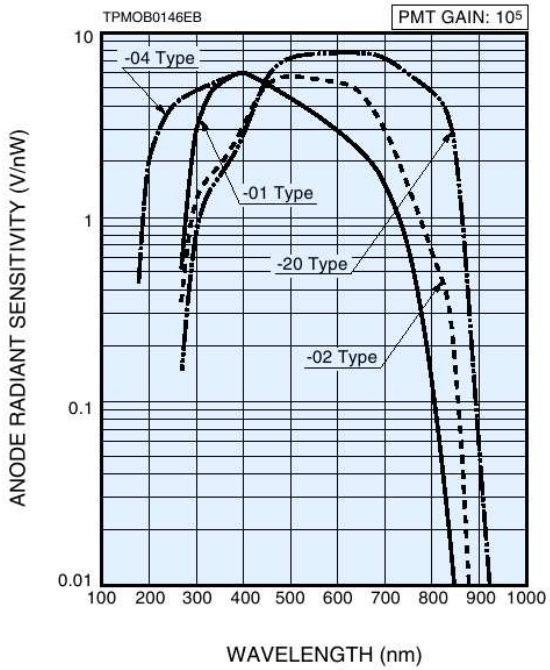

Figure 3.5: Spectral response of the Hammamatsu H6600-04 PM used in our experiments (labeled -04) together with other spectral responses of the H6600 PM family.

time to avoid degradation effects on I-V curves.

3.6 Measurement of luminance degradation

We measured emission degradation with time with a photomultiplier (Figure 3.7). Again, the Keithley multi meter was used as a digital to analog converter enabling computer data acquisition with a sampling rate of approximately three measurements per second. The OLEDS were driven at a constant voltage of 22V.

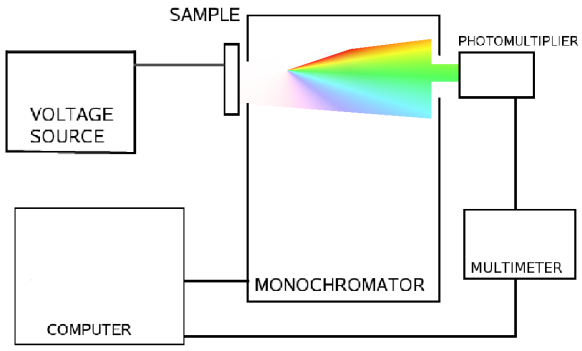

Figure 3.6: Spectrum measurement setup with a voltage source to bias the sample, a monochromator and a detector. The monochromator scans trough the wavelengths of interest while the intensities at those wavelengths are acquired.

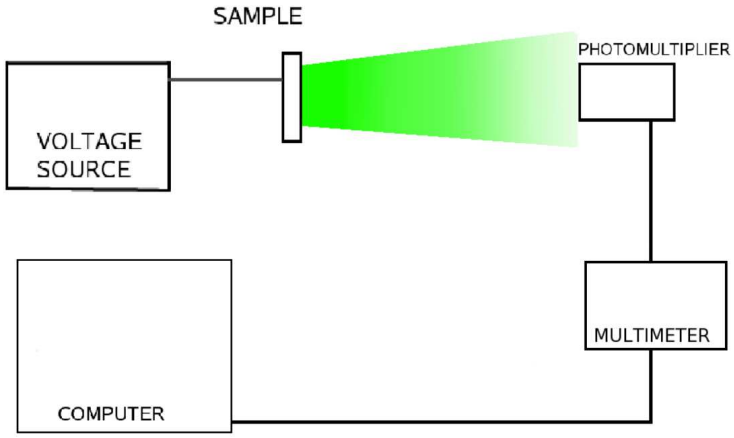

Figure 3.7: Lifetime measurement setup with a voltage source to bias the sample and a photomultiplier to detect the diminishing luminance.

Chapter 4 Growth of TPD on FTO

4.1 Introduction

In order to compare the two substrates - ITO and FTO - in terms of performance and durability we have chosen arguably the simplest and most popular OLED scheme: a two layer Alq/TPD device with an Aluminum electrode.

The structural formula of Alq and TPD and the energy level diagram are shown in figure 4.1.

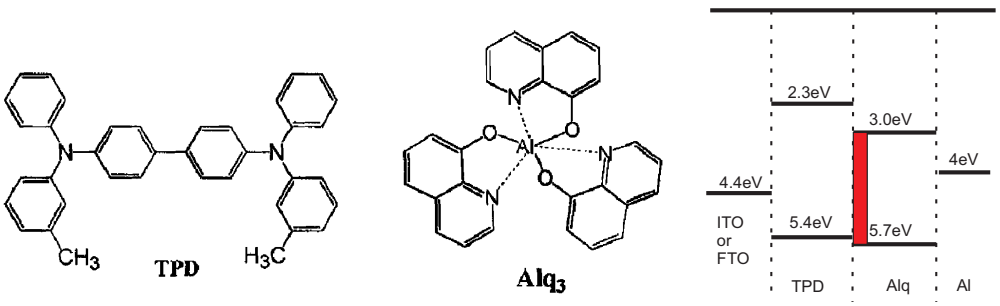

(a) (b) (c)

Figure 4.1: Structural formula of (a) TPD and (b) Alq. Part (c) shows the energy level diagram for fabricated OLEDs with ITO, FTO and Al work functions and TPD and Alq HOMO and LUMO levels. The orange area indicates the emission region which extends a few nm from the TPD/Alq interface into the Alq layer.

This device configuration has a small electron and hole barriers at the cathode/Alq and anode/TPD interface respectively. In conjunction with a relatively good hole and electron mobility, together with a good blocking organic-organic interface they are often the materials of choice for small-molecule OLEDs. They are

also commercially available. For the cathode Calcium or Magnesium would have been a better choice in terms of work function, but stability in the atmosphere was a major factor to be considered since our OLEDs were not encapsulated. For that reason, Aluminum was chosen.

For low power consumption it is desirable that the devices operate at as low voltages as possible. The layer must thus be thin enough to ensure large electric fields at low voltages, but full coverage must be accomplished to avoid leakage currents. The thickness of the layer has a low limit set by the growth mode and surface topography. The layer may grow in islands and fail to cover the whole surface or the substrate may have spikes that stick out the organic layer and make electrical contact with the cathode.

Unfortunately it turned out that while the ITO sample performed well enough to carry out measurements the FTO sample failed to work. After many repetitions, with two short lived exceptions it failed to emit light and was found to be short circuited. AFM imaging, conductive AFM imaging in particular revealed the nature of the problem. It was found that the short circuits were related to the growth mode of the organic material on FTO. Figure 4.2 shows an AFM, conductive AFM image and their superposition on of the evaporated organic materials *without* the top cathode. It is evident that the growth of both organic materials occurs in islands (Figure 4.2a). From 4.2b we can see that there are areas that have a high conductivity (bright spots). This areas proved to be ohmic since a linear I-V dependence was measured at those points, meaning that the substrate was not fully covered. Since charge mobility in metals is much higher than charge mobility in organic materials the majority of the current flows trough this exposed sites instead trough the organic layers. 4.2c shows figures 4.2a and 4.2b overlaid. It can be seen that the conductive areas lie between the islands.

Following this initial failure in fabricating OLEDs we took a step back and decided that different approach is needed. We therefore studied the growth of TPD on FTO.

4.2 Experiment

By taking an AFM image of the two substrates a considerable difference in the topography of ITO and TPD is evident (Figure 4.3). Root-mean-square roughness (RMS) values of ITO and FTO for the measured area are 1.3nm and 11nm, respectively. It has been shown that surface roughness enhances degradation and leakage currents [29, 30]. It was found that the large surface roughness of the ITO substrate induces layer inhomogeneities, especially for the vapor deposited organic layers. For organic LEDs which are entirely built up from monomeric layers, short circuits are frequently found under operation especially for thin, approximately 50 nm thick films.

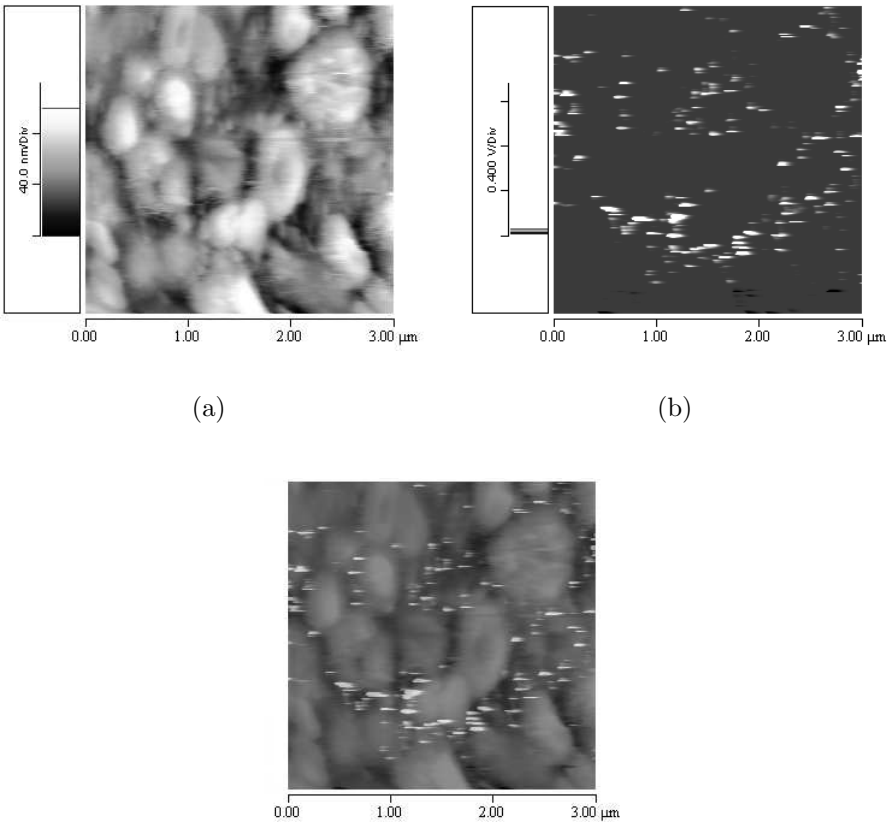

(a) (b)

(c)

Figure 4.2: Growth of TPD and Alq on FTO. Topography (a), conduction (b), superposition of topography and conduction (c). It is very well visible that high conductivity occurs between the islands (c) causing direct contact between the anode and the cathode.

To lessen the leakage currents we tried different evaporation rates as those were found to strongly influence the topography of the evaporated organic material. The island-like growth features are more likely formed at lower deposition rates. [31, 32]. Existence of the island-like features will lead to formation of electrical shorts and thus non-emissive dark spots, which are detrimental to device performance and stability. It was found that the average RMS roughness for Alq deposited on ITO at 1.33Å/s is approximately three times lower than the average RMS roughness of Alq deposited at 0.01Å/s. We prepared three samples on which 125nm TPD was evaporated at different rates: 1.4Å/s, 5.5Å/s and 8.7Å/s.

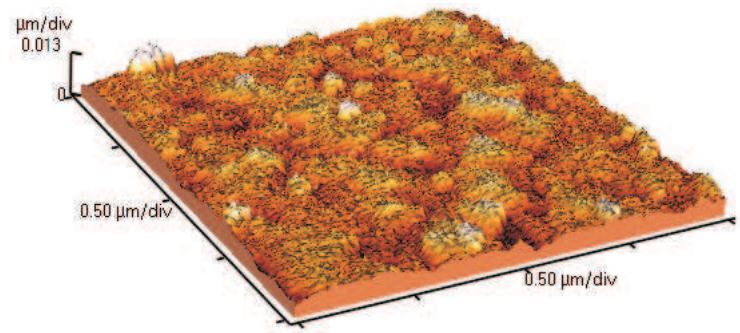

(a)

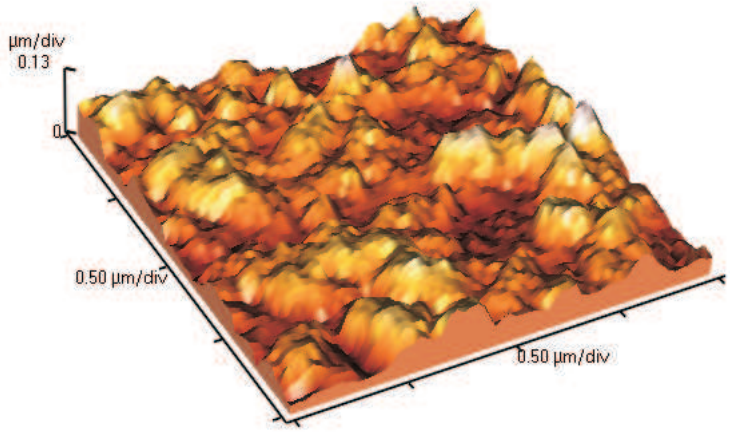

(b)

Figure 4.3: 3D view of ITO and FTO samples with contact mode AFM. A vivid presentation of the difference in surface roughness between the two samples. Note the different vertical scales.

4.3 Results

Figure 4.4 shows the TPD layer morphology. The left side column shows the topography at three different evaporation rates: 1.4Å/s, 5.5Å/s and 8.7Å/s. The dark spots correspond to bright spots on the right side column. The right side column consists of conductive AFM images, with bright spots corresponding to high current areas. This means that at the location of the dark spots, the FTO substrate comes in direct contact with the AFM tip. The depth of the holes is approximately 15nm which is enough to leave the ∼100nm FTO spikes exposed. We can see that the there is an absence of material in the proximity of the protruding spikes. Alternatively we can say that the islands form away from them. No obvious trend in coverage is visible from the AFM measurements.

Figure 4.7 shows the percentage of total area ($9\mu m^2$) trough which current density is less than 1.3nA per scan point. Each point was obtained by averaging several different scan areas on the same sample. The graph indicates that the coverage is greatest at the rate of 5.5nm/s but still unsatisfactory from the performance point of view. 1.3nA per sample point results in a current density of several tens of Amperes/cm^2. Weather AFM images for the three evaporation rates show any difference is hard to say since it is difficult to characterize the differences. However we can take coverages from individual scans and test weather the coverage distributions have a different mean. We calculate that the distributions of coverages for the three deposition rates are not different with 95% confidence level.

With ITO samples we could get relatively successful results with Alq and TPD thicknesses of 50 and 125nm respectively. It is interesting to note the differences between organic layers on FTO and ITO. Figure 4.5 shows 125nm of TPD on ITO. We can see that the scale has roughly the same interval, but there are no wide valleys with peaks which correspond to high conductivity areas as in figure 4.4. The conductive AFM image shows current variations that are much lower than those for the FTO based sample. Absolute current values can not be compared as FTO samples were measured at an AFM probe bias of 1V. For the ITO based sample we used a bias of 10V. 1V on the conductive images scale (Figures 4.4 and 4.5) corresponds to 1nA.

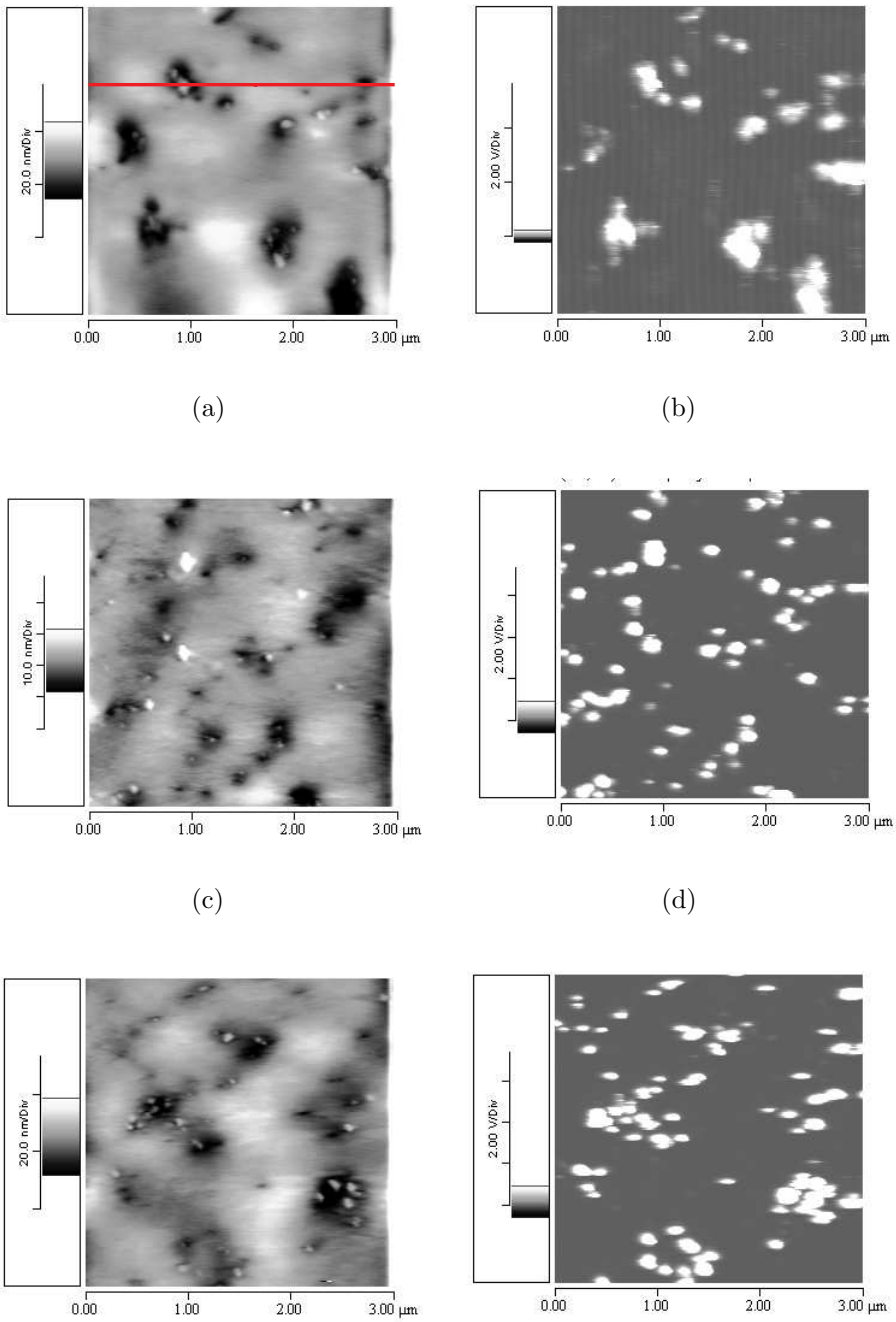

(a) (b)

(c) (d)

(e) (f)

Figure 4.4: Growth of TPD on FTO at different growth rates: (a) - topography at growth rate of 1.4Å/s, (b) - conduction at 1.4Å/s, (c) - topography at 5.5Å/s, (d) - conduction at 5.5Å/s, (e) - topography at 8.7Å/s, (f) - conduction at 8.7Å/s. The thickness measured with the quartz meter is 125nm. The red line in figure (a) represents the cross section line. The cross section is shown in figure 4.6.

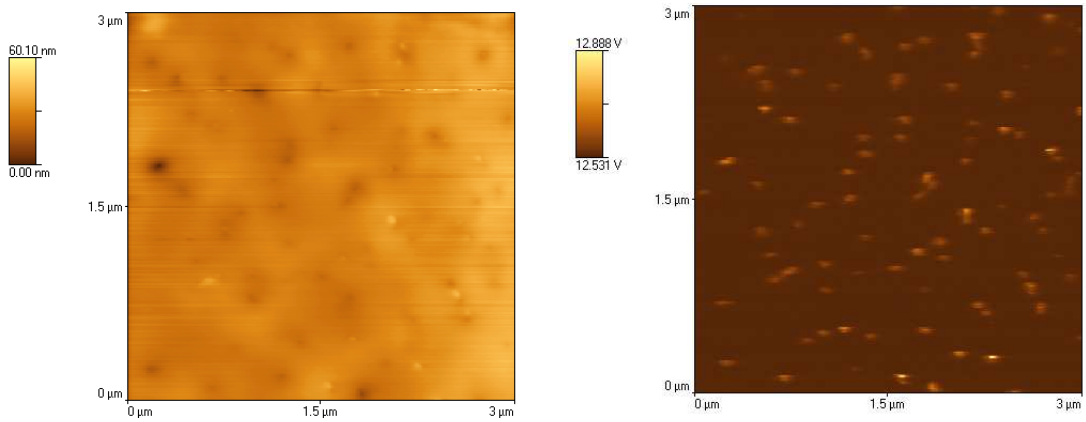

(a) (b)

Figure 4.5: ITO based sample with 125nm of TPD. (a) topography, (b) conduction AFM. In contrast to FTO based sample there are not any spikes visible. Conductive AFM shows a smaller current variation on the ITO based sample. 1V on the scale coresponds to 1nA

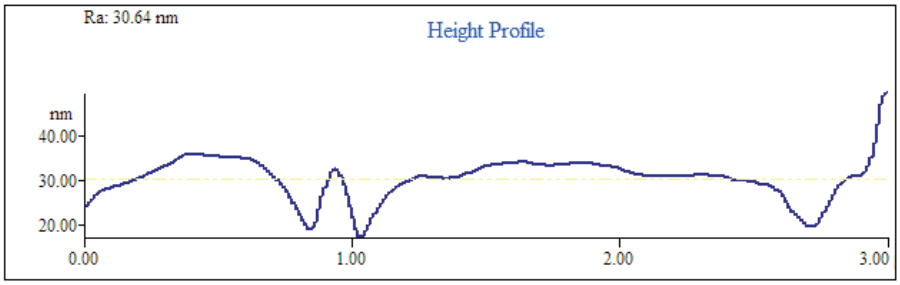

Figure 4.6: Profile from figure 4.4a. The peak at approximately 1μm is visible as a bright spot in the current window implying that it corresponds to the FTO peak. This is consistent with surface roughness of FTO (figure 4.3) and TPD surface thickness (125nm)

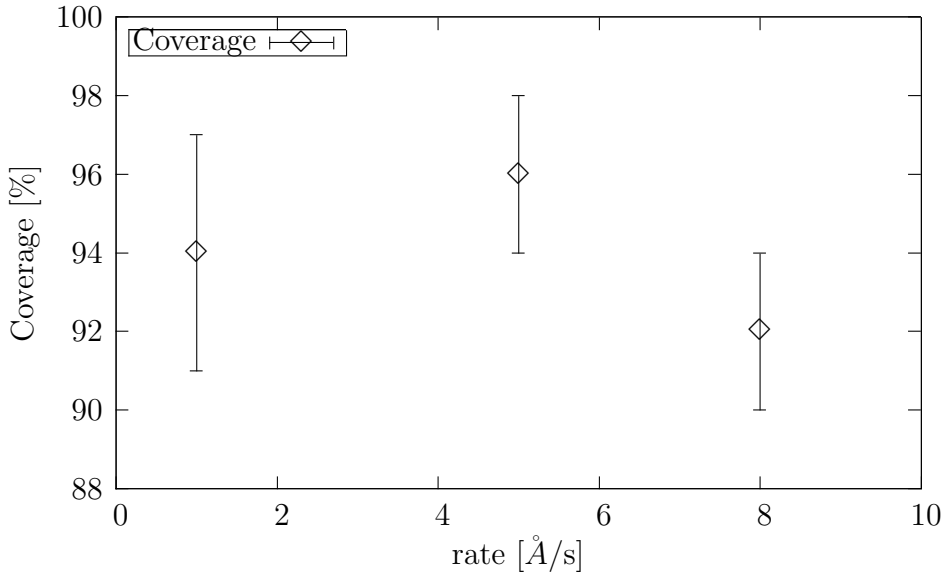

Figure 4.7: Percentage of covered area vs. evaporation rate for threshold current of 1.3nA. Highest coverage is achieved at the rate of 5.5nm/s but still unsatisfactory from the performance point of view.

Chapter 5 ITO and FTO substrate comparison

5.1 Introduction

After learning that evaporation rate does not have the wanted effect on TPD coverage of FTO, the simplest approach was to manufacture OLEDs with larger thicknesses of organic material at the expense of larger biases.

5.2 Experiment

We increased the thickness of TPD to 170nm and kept the Alq thickness 50nm as before. TPD was evaporated at 9.6Å/s and Alq at 2Å/s. All the other parameters (etching, cleaning procedure) remained the same as were when non functional FTO based OLEDs were prepared. Immediately after the samples were taken out of the UHV chamber I-V measurements and subsequently spectroscopic and lifetime measurements were performed. Throughout this chapter the ITO/TPD/Alq/Al OLED will be referred to as the ITO sample whereas the FTO/TPD/Alq/al OLED will be referred to as the FTO sample.

5.3 Results and discussion

5.3.1 Current voltage characteristics

To explain the I-V characteristics we turn to continuum model equations in chapter 2. We consider the following specific features of our device configuration. The contacts can be considered ohmic leaving the bulk properties of the organic materials govern the I-V characteristics [35]. Furthermore TPD has a sufficiently high hole mobility to allow rapid hole transport from the anode to the TPD/Alq interface.

The transport is therefore unipolar, governed by Alq properties alone, with ohmic contacts at the TPD/Alq and Alq/Al interfaces. Nearly all the voltage drop occurs in the Alq layer. We can thus consider that the voltage applied to the OLED is applied to the Alq layer and electrons solely contribute to the current. The recombination zone in Alq is narrow in comparison with the Alq thickness.

5.3.2 Unipolar charge transport

Any voltage U maintained between the cathode and the anode is accompanied by an electric field within the semiconductor placed between them - inducing a current J. At very low injection levels the injected charge is much less than the free carrier density already present in the semiconductor. In the case of ohmic contacts, for one dimensional scheme, the internal uniform electric field governs the conduction as [43]:

$$J = qn_0\mu F$$

where $F = \frac{U}{d}$, U being the applied voltage, and d the layer thickness

When the injection levels rise with the rising applied voltage the injected charge is no longer small in comparison with the background charge and the material is no longer neutral. The accumulated charge alters the electric field distribution and thus the total current. In the case that the injected carrier density is much larger than the thermal charge density the continuity and the Poisson equation have the following form:

$$J = qn_{inj}(x)v(x) \tag{5.1}$$

$$\frac{dF(x)}{dx} = \frac{qn_{inj}(x)}{\epsilon\epsilon_0} \tag{5.2}$$

Realizing that $v = -\mu F$ and applying the boundary condition $F(0) = 0$ the solution for equations 5.1 and 5.2 is:

$$J = \frac{9}{8}\epsilon\epsilon_0\frac{U^2}{d^3} \tag{5.3}$$

Equation 5.3 is referred to as the Mott-Gurney law, Child's law for solids, or the trap-free square law. The conduction regime is referred to as space charge limited conduction (SCLC).

Not all carriers that are injected in the bulk material contribute to the conduction. In the case trap states are present, many injected electrons will be trapped, and will not contribute to the total current. However, they will contribute to the voltage drop across the material. This will yield a different conduction regime called trap charge limited conduction (TCLC).

For TCLC the current is given by [1]:

$$J_{TCLC} = k\frac{V^{l+1}}{h^{2l+1}} \tag{5.4}$$

Where h is the Alq thickness, $l = E_t/k_bT$, E_t being the characteristic trap energy and

$$k = N_c\mu q\left(\frac{\epsilon\epsilon_0}{N_t q(l+1)}\right)^l\left(\frac{2l+1}{l+1}\right)^{l+1}$$

where N_c is the density of states in the conduction band, μ is the mobility, q the unit electric charge, ϵ the dielectric constant, ϵ_0 the vacuum permittivity and N_t trap density.

We observed TCLC conduction in the range $U > 5$V (Figure 5.1) with $l+1$ =4.4 and $l + 1 = 2.3$ for the ITO and FTO sample respectively.

At lower voltages ($U < 4$V) conduction appears to be between ohmic SCLC as $l_{ITO} + 1$ =0.6 and $l_{FTO} + 1$ =1.1 for the ITO and FTO sample respectively. We seen se that the nature of conduction of ITO sample is closer to ohmic than that of the FTO sample.

The accuracy and error estimation of the I-V characteristic is compromised by *anomalous behavior* reported to occur at low voltages [1]. At the low voltage end of the I-V curve we observe a quantitatively unreproducible behavior. This phenomena was also observed by us and is shown in figure 5.2. We can see that the I-V curve is not continuous but has segments of negative differential resistance (NDR) around 8 and 15V. At those voltage segments visible emission at localized spots was observed. The spectra is material independent, broad and mostly in the infrared, therefore unlikely caused by an electronic transition. From this it was concluded that in NDR regime the vast amount of total current flows trough *localized pathways* - corresponding to emission spots. Since we are interested in the transport trough homogeneous organic layers we tried to avoid this conduction mode. This was done by restricting ourselves to parts of the I-V graph where NDR does not occur. Also when current switches to localized pathways homogeneous emission vanishes [44]. In our case NDR occurs also above 10V. This is also the reason why our I-V curves are limited to that value.

We thus fitted the lower part of the I-V characteristics with a model of the form:

$$I = p_1V^{p_2} \tag{5.5}$$

Where $p1$ and $p2$ largely unknown parameters.

We expected similar I-V curves for the two samples. The work function of ITO depends strongly on the cleaning procedure and can reportedly assume values between 4.1 to 5.53eV [33]. For the case of our cleaning procedure it is reported to

be equal to 4.4eV. The work function of FTO is less dependent on the cleaning procedure, and is also equal to 4.4eV. Since every other aspect of the two OLEDs is identical, the enormous difference in current densities between the two samples, evident in figure 5.1, comes somewhat unexpected. We believe that surface roughness can be held responsible for this discrepancy.

Surface roughness of FTO is considerably greater than that of ITO (Figure 4.3) which implies that the roughness of the on-top evaporated materials will be also different [34]. This means that the thickness will vary throughout the sample. Figure 5.3 shows the cross-sections of the Alq layer for the ITO and FTO structure. The cross-section was calculated by calculating the thickness at each point as:

$$h_{alq} = h_{nom} - h_{Alq} + h_{TPD} - mean_{TPD} + mean_{Alq}$$

where h_{nom} is the nominal (average) Alq thickness of 50nm, h_{Alq} and h_{TPD} are the raw AFM heights while $mean_{TPD}$ and $mean_{Alq}$ are the mean raw AFM heights of the contact/Alq and Alq/TPD interface respectively.

If we assume that the thickness varies so slowly that one-dimensionality from which transport equations are derived is not violated, we can define an effective thickness h_{eff} which corresponds to the uniform thickness throughout the sample that would yield the same I-V response as the varying thickness in the rough sample. The condition seems to be violated judging from figure 5.3. But if we set h and x scales equal we see that the highest surface slopes are below 20°. From this we deduce that the direction of the electric field does not deviate substantially from the parallel plane field. It remains unchecked how this approximation is correct, but we bare in mind that we are only interested in explaining the two orders of magnitude different currents between the ITO and FTO based samples. Thus we can calculate the total current as the integral of all partial currents at each surface element holding all surface elements parallel.

$$I = \int_S k \frac{V^{l+1}}{h^{2l+1}} \, dS \tag{5.6}$$

Which is in our case approximated by a sum of currents over the sample at each sampling point.

$$I = \sum_{i=1}^{N} k \frac{V^{l+1}}{h_i^{2l+1}} \, dS \tag{5.7}$$

We define the effective thickness as:

$$h_{eff} = \left(N \frac{1}{\sum_{i=1}^{N} \frac{1}{h_i^{2l+1}}} \right)^{\frac{1}{2l+1}} \tag{5.8}$$

Computing the effective thickness h_{eff} for the nominal Alq thickness of 50nm for ITO and FTO samples we get h_{ITO}=48nm for ITO and h_{FTO}=11nm for the FTO sample. This has a great influence on the current-voltage curve as a $\frac{1}{5}$ ratio of the effective thickness yields a ratio of 200 in the current densities for l=2.2. Also: from figure 5.1 we can see that low voltage conduction regime is closer to ohmic for the ITO sample. This is consistent with a greater effective thickness for ITO as thick Alq films (>30nm) show ohmic conduction at low voltages, whereas thin films (<30nm) show SCLC [35]. It is interesting to note that the effective thickness will always be smaller for a rough sample. The effective thickness is greatest for a completely smooth layer. In that case it is equal to the average thickness. This can be seen from equation 5.6. We are looking for a function $h(x)$ so that 5.6 will be minimized. From calculus of variation this yields

$$k\frac{U^{l+1}}{h^{2l+1}} = const$$

since k, U, and l are constants $h(x)$ must be constant.

Surface roughness also influences the morphology which in turn influences the characteristic decay energy [26] yielding a different exponent l in equation 5.4.

5.3.3 Electroemission spectroscopy

Figure 5.5 shows normalized electroemission spectra for the ITO and FTO sample. As expected, the spectra are nearly identical since the spectrum is entirely determined by electroluminescent properties of Alq. If TPD would also exhibit electroluminescence one would expect a voltage dependence of the spectrum as the recombination zone at the Alq/TPD interface would shift [36]. This was not observed by our measurements. Figure 5.6 shows 5 normalized spectra of an ITO based sample. The spectra were measured at 10, 12, 14, 16, and 18V.

5.3.4 Lifetime

The main purpose of this thesis was to see if the absence of Indium in the FTO substrate has any notable influence on the lifetime of OLEDs. It has been reported [10, 11] that an initially flat cathode surface degrades in several stages. The initial stage is characterized by local distortions of the cathode surface. With operation time other features can appear, followed by "explosions" that disrupt the cathode. The evolution of domelike structures has been studied by scanning photoelectron microscopy (SPEM) [13]. SPEM allows quantitative chemical mapping of the cathode surface and underlying hole transport and ITO film. The method is also sensitive to surface topography because of the grazing geometry or he electron analyzer with respect to the sample surface plane. SPEM measurement have

shown in In 3d map that ITO surface is locally exposed at the cathode fracture. In deposition are present on the fracture edges and on the surrounding intact cathode structure. The organic film is destroyed.

In addition to Indium diffusion into organic layers other mechanisms contributing to luminance decay have been documented. They contribute to electroluminescent decay on various time scales. We will give an incomplete list of this processes in order to comment the measured lifetimes of the two samples.

Ion migration

It is believed that mobile ions are present in the organic layers of as-fabricated OLEDs [6, 7, 37]. These ions migrate under the influence of the external applied electric field and arrange in such way that they decrease the effective electric field or/and increase the carrier injection barrier. This type of degradation is mostly on the timescale of minutes and is reversible by application of reverse bias.

Dark spot formation

Dark spots are for nonemissive areas that appear at fabrication and grow in the presence of oxygen and water until they eventually cover the entire emissive area [39, 40]. Water and oxygen find their way to the organic material trough pinholes in the cathode formed because of shadowing effects. One of possible shadowing situations is shown in figure 5.7.

An asperity or a particle unintentionally deposited during or after cleaning as well as an organic chunk deposited during evaporation will cause entry point for oxygen and water by exposing the organic layers. Such exposures are the center of the growing nonemissive areas, caused by the delamination of the cathode from the organic layers. This undesired phenomena can be avoided by encapsulating the device in an inert atmosphere. Figure 5.8 show such particle easily visible after the deposition of the cathode. No matter what care the samples were prepared with, this particles, suspectedly originating from air could never be avoided.

Luminance degradation

The part of the emitted area that remains outside the dark spots undergoes a luminescent decay caused by increase of internal resistance and decrease of electroluminescent efficiency. Luminance decay is temperature dependent [41]. It is believed that local short circuits caused by spikes of the substrate or shadowing effects are responsible for local hot spots that in the presence of water and oxygen alter the chemical structure of the organic layers [5].

Figure 5.9 shows the luminance versus time for the FTO (solid line) and ITO (dotted line) based OLEDs driven at 22.8V. The halflifes for ITO and FTO based

sample are 269 and 202s respectively. We can see that the luminance of the FTO sample is roughly twice as large as that of the ITO sample while the current trough FTO sample is ∼50 times larger. This implies a much lower quantum efficiency for the FTO sample. This cannot be explained with leakage currents as leakage currents would manifest themselves in an ohmic I-V dependence. Incomplete Alq coverage on TPD would explain a larger current, while a broad Alq thickness distribution would explain the increased luminance. Figure 5.10 illustrates this situation. The HTL-ETL interface is drawn straight for simplicity, lateral dimensions have been shrunk. In the center we see the absence of ETL: Alq. Holes can flow directly to the cathode. At the left and right sides we can see the beginning of two chunks of Alq. The light output generated at the HTL-ETL (TPD-Alq in our case) interface will be greater than as if an average thickness would occupy the same area because of the $\frac{1}{d^{2l+1}}$ thickness dependence of the TCLC current density. If this is true, our model explaining the current discrepancy between the FTO and ITO sample is wrong. Another explanation could be that a different morphology produces new states that allow a non-radiative exciton decay.

For better comparison between decay mechanisms we normalize the decay curve in luminescence and time. The result is seen in figure 5.11. We see that the shapes of the curves are slightly different implying different relative contribution of multiple degradation mechanisms [41]. The degradation function can be fitted with three exponential functions with different time constants τ and relative amplitudes A in the form of:

$$I = A_1 \exp(-\frac{t}{\tau_1}) + A_2 \exp(-\frac{t}{\tau_2}) + A_3 \exp(-\frac{t}{\tau_3})$$

The results are given in table 5.1. We can see that the three time constants are of the same order of magnitude for each degradation process. Since the degradation of both ITO and FTO sample can be modeled with a three exponential function we expect that the same physical processes are involved and thus rule out indium diffusion. Also, lifetimes of more than 10000 hours are reported on ITO samples meaning that the diffusion of ITO occurs on much larger timescales.

It is interesting to note that the same experiment performed on a Alq only OLED yields a time dependent luminance decay that can be fited with four exponential functions [42]. In Alq the degradation is associated to the formation of different species that have different protection from external agents by means of different molecule packing. We believe that TPD degradation overshadows at least some of deterioration processes in Alq impeding us to see all four exponential contributions reported. Since TPD and Alq are connected in series a fast degradation process in one layer would overshadow occurrence of large time scale processes the other. TPD in fact shows inferior morphological stability than Alq.

Figure 5.12 shows the portion of the still luminescent area (white). The square represents the initial luminescent area. The pictures have been taken with a CCD

ITO sample		
process	relative contribution A	time constant τ
1	0.32	0.022
2	0.38	0.13
3	0.29	1.29

FTO sample		
process	relative contribution A	time constant τ
1	0.55	0.035
2	0.18	0.20
3	0.26	1.64

Table 5.1: Degradation parameters for ITO and FTO sample. For both samples we can see three distinct time constants of exponential decay.

camera and an intensity threshold has been set with a picture editing software to discriminate between the emissive and nonemissive area. We can see that black spot formation is a major reason for our OLED degradation leaving after one hour of operation (a few hour of exposure to atmospheric conditions) only about 30% of emissive area on the ITO sample and about 40% on the FTO sample.

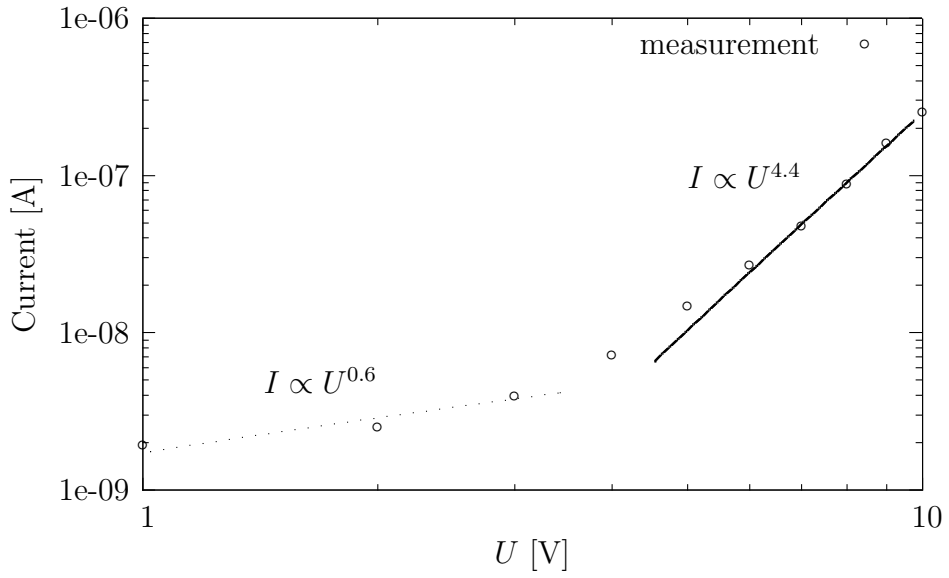

(a)

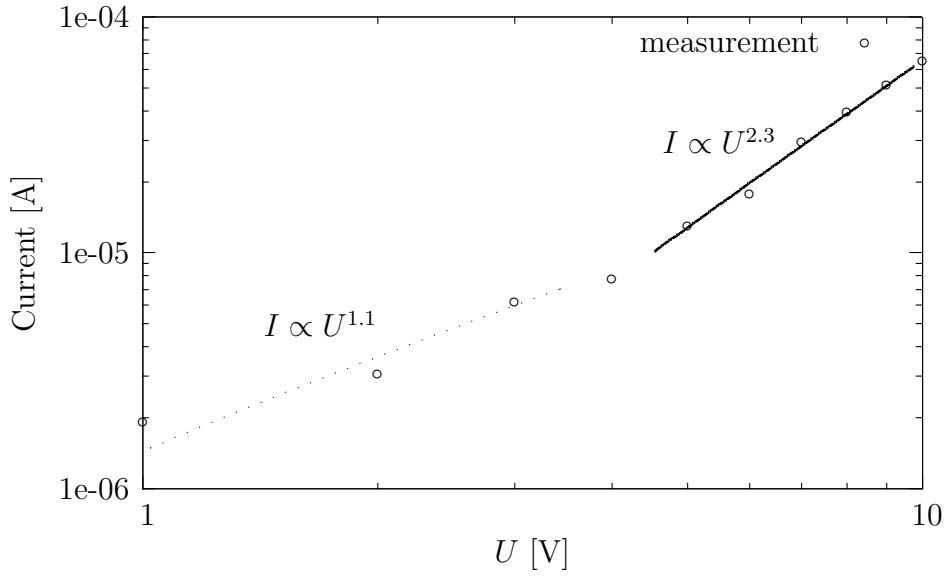

(b)

Figure 5.1: Current-voltage measurements (dots) for the ITO (a) and FTO (b) sample in forward bias and corresponding fits (solid and dotted line). The model used to fit data was TCLC (solid line) and SCLC (dotted line)

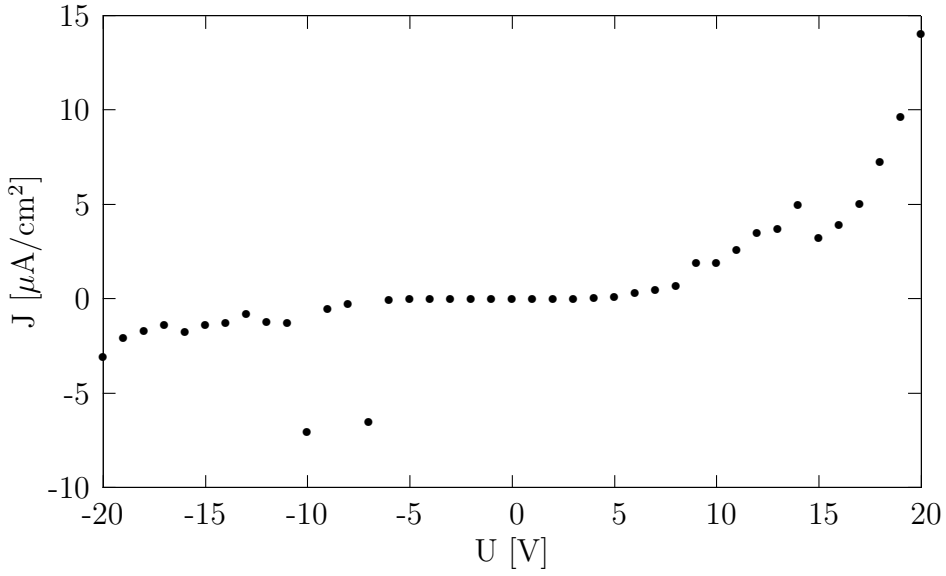

Figure 5.2: A representative graph *anomalous I-V characteristics*. Instead of continuous rise of current with voltage negative differential resistance (NDR) often occurring during an I-V scan. Such NDR can be seen around 15V as well as in the negative part of the graph.

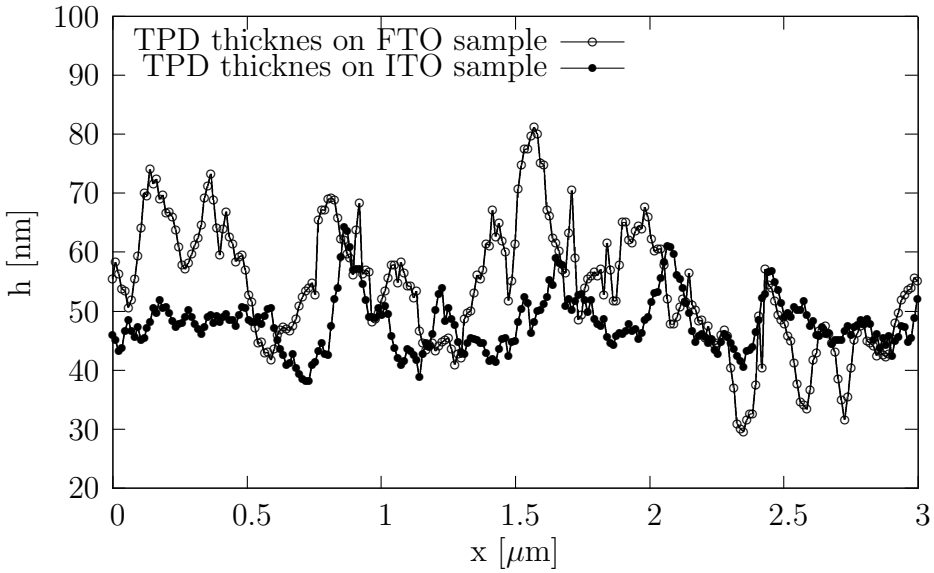

Figure 5.3: A cross section of thickness variation for FTO (empty circles) and ITO (filled circles) sample. The thickness varies more than 50% the average thickness, but the slope of the of the organic film never exceeds 20° and is usually much less. This allows us to assume that the electric field lines are almost parallel and calculate the current as the sum of currents trough each surface section

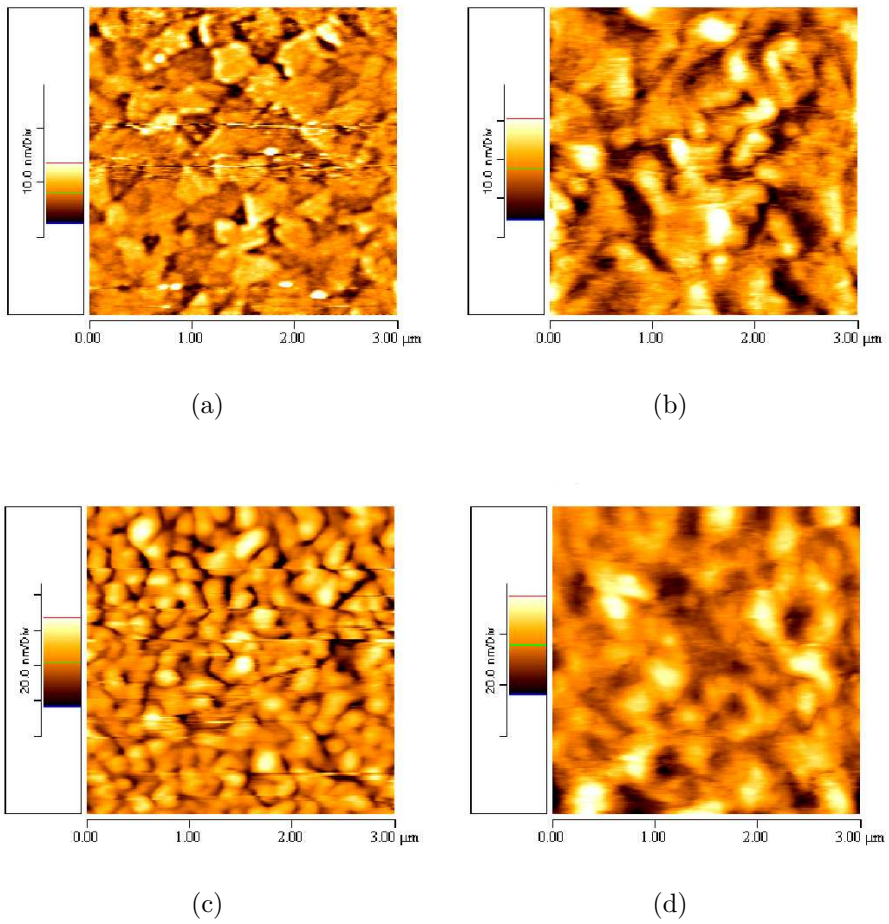

Figure 5.4: Topography of: (a) - ITO sample - TPD, (b) - ITO sample - Alq on TPD, (c) - FTO sample - TPD, (d) - FTO sample - Alq on TPD

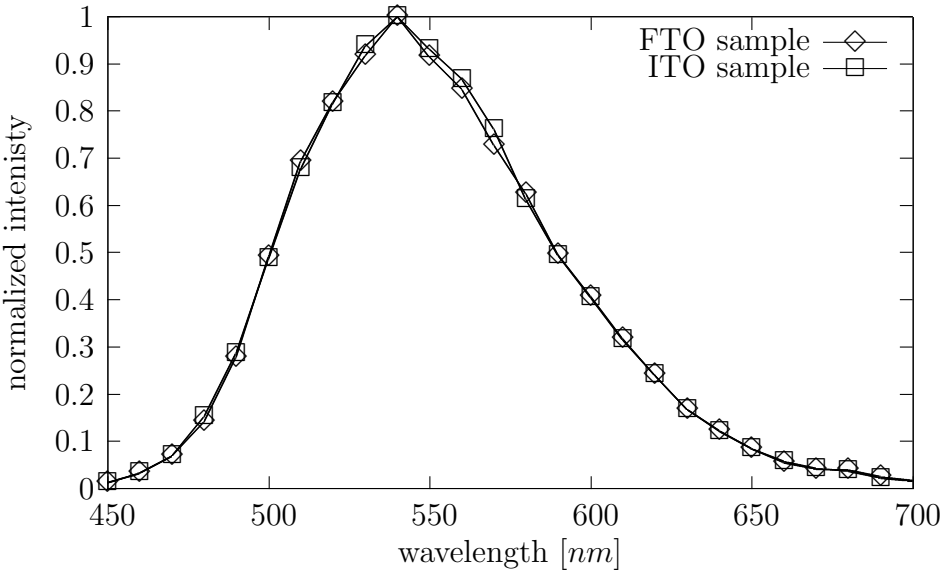

Figure 5.5: Normalized spectra of the FTO based (diamonds) and ITO based (squares) sample.

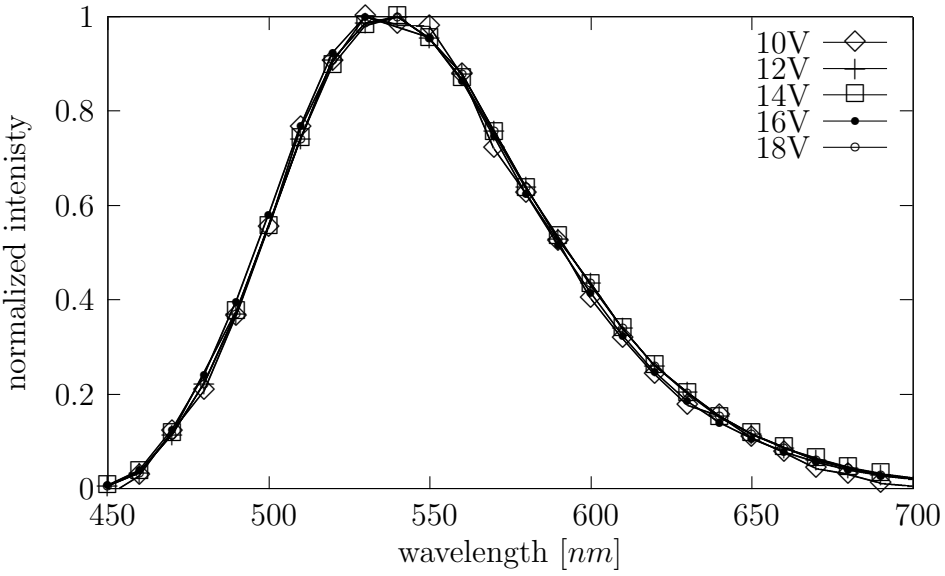

Figure 5.6: Five normalized spectrums for the ITO based sample biased at 10, 12, 14, 16 and 18V. The spectrums are not shifted implying electroluminescence occurs in Alq only. If recombination occurred also in the TPD layer a shift would be noticed [36].

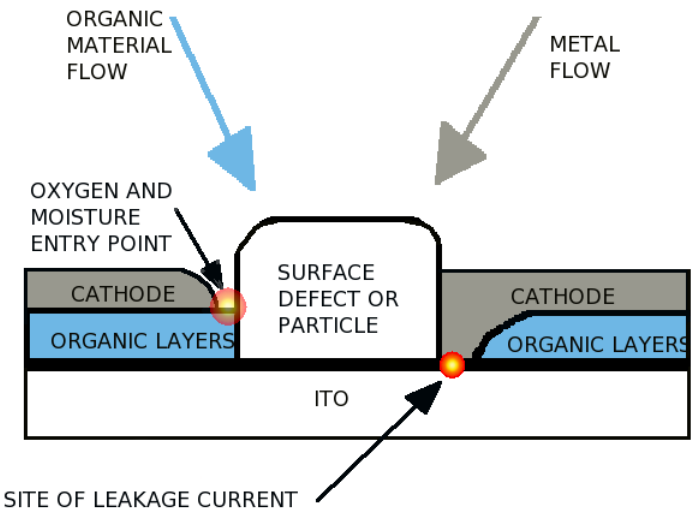

Figure 5.7: Shadowing effect at an asperity, a particle or an organic chunk deposited during evaporation. Such a particle that is thicker than the layers of the OLED will cause an entry point for water and oxygen. It may also be the source of local short circutis.

Figure 5.8: Relatively large particles on the cathode after sample preparation. The possible source of oxygen and water entry points and local short circuits. The side of the square is approximately 4mm.

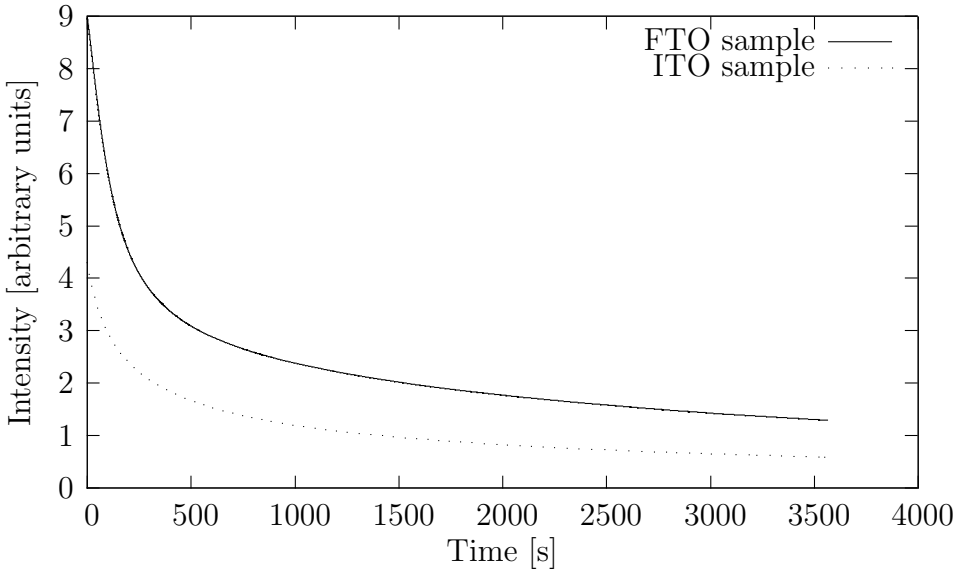

Figure 5.9: Luminance decay versus time for FTO (solid line) and ITO (dotted line) based sample.

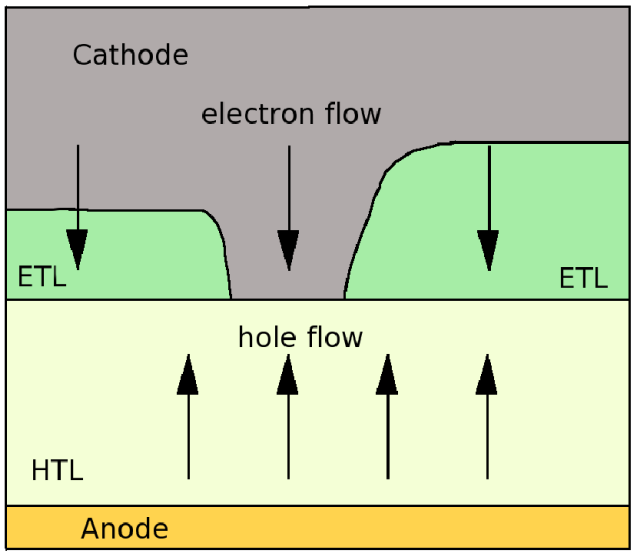

Figure 5.10: Possible current routes. Holes can flow from the anode to the cathode directly trough the hole transpost layer (HTL) and increase the current while a non uniform thickness distribution of the electron transpost layer (ETL) thickness results in greater light output.

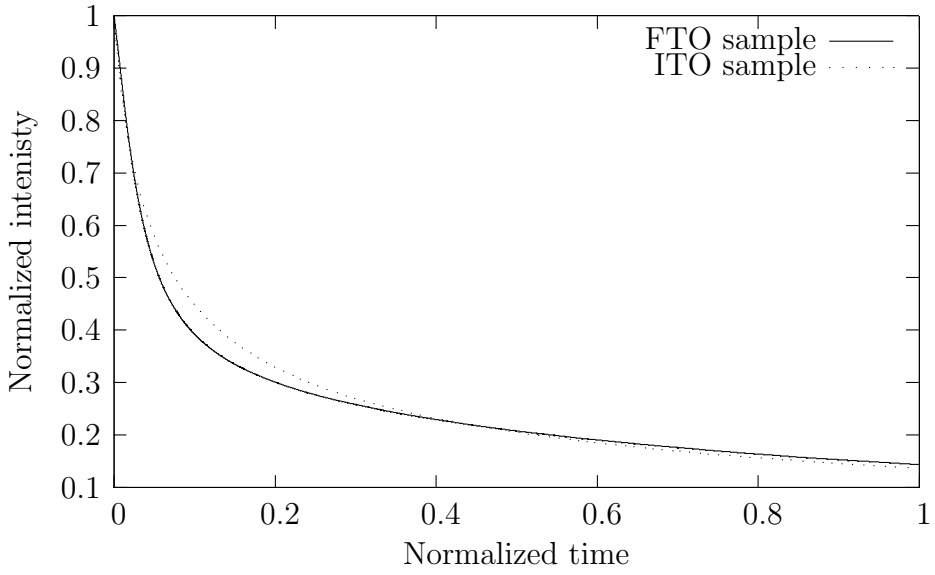

Figure 5.11: Normalized intensity versus normalized time for FTO (solid line) and ITO (dotted line) based sample.

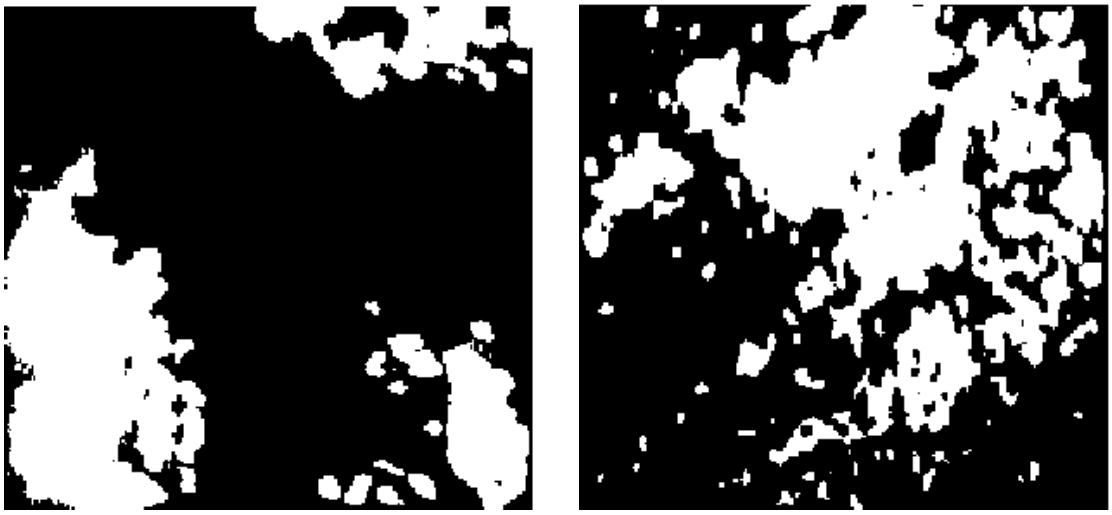

(a) (b)

Figure 5.12: Portion of still emissive area (white) and portion of the "dead" area (black) after an hour of operation and approximately 3 hours of air exposure. The picture was made with a CCD camera and edited in a picture editing software to discriminate between the emissive and nonemissive area

Chapter 6 Conclusions

With atomic force microscopy we confirmed that TPD and Alq grow in islands and full coverage can not be achieved over our range of evaporation velocities until a certain thickness is evaporated. The thickness needed for satisfactory coverage was found to be relatively large in comparison to standard OLED thick nesses.

Regarding lifetime we can say that there are different degradation mechanisms between the ITO and FTO sample. It is very unlikely that ITO diffusion is responsible for luminance degradation on observed timescales as lifetimes of several thousand hours have been reported on ITO substrates. The degradation was most likely governed by morphological changes of the organic layers.

Unfortunately in the timeframe given for the experiments, these two were the only successful specimens. Out of twenty pairs made only the last two FTO based samples actually worked. With only the last one surviving the whole measurement process. For this reason there is no way of knowing to what extent the curves are reproducible.

In the light of current knowledge we would have done things differently. Firstly a smoother FTO would be sought. Ideally it would have the similar roughness as ITO. With similar roughness we mean fairy similar standard roughness parameters such as: root-mean square, peak to valley and average roughness. Secondly, samples would be plasma etched to further smoothen the surface and/or a thin layer of copper phthalocyanine (CuPc) would be applied to smoothen the surface of the anode. Third, although harder to implement, would be to test our samples in the absence of oxygen and water. Two things would be accomplished by this. First, with equal smoothness of the substrates the unwanted geometry influence would be reduced. Second, slower degradation processes such as our indium diffusion is expected to be, would not be buried in faster processes. We belive that the absence of the forementioned steps together with testing these samples in atmospheric conditions, ie. not using any encapsulation, carries the responsibility for the halflifes 5 orders of magnitude smaller than most reported OLEDS. The lifetime difference is however 2 orders of magnitude than comparable nonencapsulated devices [4].

A more profound difference than luminance-time is observed in the current-voltage characteristics between the two samples. The currents trough the FTO based samples are orders of magnitude larger than currents trough the ITO based sample. We attributed this difference to FTO's surface roughness. Despite the very different currents the halflifes are very similar. From this we can conclude that the main degradation process was not bias dependent. This leads us to think that bias independent growth of black spots was the main source of degradation of our devices. The spectra were as expected similar dependent only on the HOMO LUMO states of Alq. There is no noticeable dependence of the emission spectrum from the choice of substrate. Weather there is a dependence on roughness or cleaning treatment or other parameters remains unknown as the only parameters changed were film thickness and deposition rate. However there is a strong dependence of cleaning treatment and/or substrate on luminance decay was noticed. ITO based samples were $\sim$80% successful - successful meaning that they showed halflifes in the range of minutes. The remaining portion extinguished in a matter of seconds or immediately in a burst of life. We attribute this to large visible particles similar to those depicted in figure (5.8) When such a particle was large enough to be easily recognized by brief eye inspection the sample would invariably be shorted after deposition.

Bibliography

[1] W. Brütting, S. Berleb, A. G. Muckl, *Device physics of organic light-emitting diodes based on molecular materials*, Organic Electronics 2 (2001) 143.

[2] L. S. Hung, C. H. Chen, *Recent progress of molecular organic electroluminescent materials and devices*, Material Science and Engeneering R39 (2002) 143-222.

[3] S. H. Kwon, S. Y. Paik, J. S. Yoo, *Electroluminescent properties of MEHPPV light-emitting diodes fabricated on the flexible substrate*, Synthetic Metals 130 (2002) 5560.

[4] D. Davidov *et al.*, *Degradation of nonencapsulated polymer-based light-emitting diodes: Noise and morphology*, Applied Physical Letters 71 (1997) 23.

[5] F. Papadimitrakoloulos, X. M. Zhang, D. L. Thomsen, K. A. Higginson, *A chemical faliure mechanism for Aluminium(III) 8- Hydroxyquinoline Light-Emitting Devices*, Chemistry of Materials, 8 (1996) 1363-1365.

[6] P.Cusumano, F. Burita, A. Di Cristofalo, C. Cali *Efect of driving method on the degradation of organic light emitting diodes*, Synthetic Materials, 139 (2003) 657-661.

[7] D. Zou, M. Yahiro, T. Tsutsui, *Improvement of Current-Voltage Characteristics in Organic Light Emittin Diodes by Application of Reversed-Bias Voltage*, Japanese Journa of Applied Physic, 37 (1998) L1406-L1408.

[8] C. W. Tang, S. A. VanSlyke, *Organic electroluminescent diodes*, Applied Physical Letters 51 (1987) 913-915

[9] C. N. Li, A. B. Djurišić, C. Y. Kwong, P. T. Lai, W. K. Chan, S. Y. Liu, *Indium tin oxide surface treatments for improvement of organic light-emitting diode performance* Applied Physics A 80 (2005) 301-307.

[10] *Flourine tin oxide as an alternative to indium tin oxide in polymer LEDS* A. Anderson, N. Johansson, P. Bröms, N. Yu, D. Lupo, W. R. Salaneck

[11] A. R. Schlatmann, D. Wilms Floet, A. Hilberer, F. Garten, P. J. M. Smulders, T. M. Klapwijk, and G. Hadziioannoub, *Indium contamination from the indium-tin-oxide electrode in polymer light-emitting diodes* Applied Physics Letters 69 (1996) 1764-1766

[12] A. C. Arias, J R. de Lima, I. A. Hümmelgen, *Tin Oxide as a Cathode in Organic Light-Emitting Diodes*, 10 (1998) 392-394.

[13] L. Gregoratti et all, *Mechanism of dark-spot degradation of organic light-emitting devices*, 86 (2005)

[14] C. Chao, K. Chuang, S. Chen, *Failure phenomena and mechanisms of polymeric light emitting diodes: Indium-tin-oxide damage*, Applied Physics Letters 69 (1996) 2894-2896

[15] R. Lessman, I. A. Hümmelgen, *Thin Copolymer-Cased Light-Emitting Display Made with Fluorine-Doped Oxide Substrates*, Materials Research 7 (2004) 467-471.

[16] J. C. Scott, G. G. Malliaras, *Charge injection and recombination at the metal-organic interface*, Chemical Physics Letters 299 (1999) 115

[17] A. B. Walker, A. Kambili, S. J. Martin, *Electrical transport modelling in organic electroluminescent devices*, Condensed Matter 14 (2002) 9825-9876.

[18] J. Singleton *Band Theory and Electronic Properties of Solids* (Oxford: Claredon)

[19] S. M. Sze, *Physics of Semiconductor Devices*, New York, 1981.

[20] P. S. Davids, I. H. Campbell, D.L. Smith, *Device model for single carrier organic diodes*, Journal of Applied Physics 82 (1997) 6319

[21] C.D.J. Blades, Alison B. Walker, *Simulation of light-emitting diodes*, Sythetic Metals 111-112 (2000) 335-340.

[22] M. Pope, C. E. Swensberg, *Electronic Processes in Organic Crystals and Polymers*, New York 1999.

[23] K. Yase a, Y. Yoshida, S. Sumimoto, N. Tanigaki, H. Matsuda, M. Kato, *Aggregation mechanism of triphenyldiamine*, Thin Solid Films 273 (1996) 218-221.

[24] H. Frolich, G. L. Sewel, Proceedings of the Physical Society 74 (1959) 643.

[25] W. Shockley, W. T. Read Jr., *Statistics of the Recombination of Holes and Electrons* Physical Review 87 (1952) 835

[26] R. Scmechel, H. von Seggern *Electronic traps in organic transport layers*, Physica Status Solidi, 201 (2004) 1215-1235.

[27] A. M. Bernardus, *Chemical vapour deposition of tin oxide thin films* Technische Universiteit Eindhoven, 2003. ISBN 90-386-2715-7

[28] G. Binning, C.F. Quate, *Atomic Force Microscope*, Physical Review Letters 56 (1986) 930-933

[29] CH. Jonda, A. B. R. Mayer, U. Stolz, *Surface roughness effects and their influences on the degradation of organic light emitting diodes*, Journal of Materials Science 35 (2000) 5645-5651

[30] K. Kim, Y. Tak, Y. Han, K. Baik, M. Yoon, M. Lee, *Relationship between Surface Roughness of Indium Tin Oxide and Leackage Current of Organic Light-Emitting Diode* 42 (2003) L438-L440

[31] C.B. Lee, A. Uddin, X. Hu, T.G. Andersson, *Study of thermal evaporation rate effects on the OLED*

[32] L.F. Cheng, L.S. Liao, W.Y. Lai, X. H. Sun, N. B. Wong, C. S. Lee, S. T. Lee, *Effect of deposition rate on the morphology, chemistry and electroluminescence of tris-(8-hydroxyquinoline) aluminum films*

[33] Y. Park, V. Chong, Y. Gao, B. R. Hsieh, C. W. Tang, *Work function of indium tin oxide transparent conductor measured by photoelectron spectroscopy*, Applied Physics Letters 68 (1996) 2699-270

[34] E. Han, L. Do, N. Yamamoto, M. Fujihira *Crystalization of organic thin films for electroluminescent devices* Thin Solid Films 273 (1996) 2002-2008

[35] P. E. Burrows, Z. Shen, V. Bulovic, D. M. McCarty, S. R. Forrest, *Relationship between electroluminescence and current transport in organic heterojunction light-emitting devices*,J. Appl. Phys. 10 (1996) 79.

[36] Z. H. Kafafi *Organic Electroluminescence*, CRC Press 2005

[37] J. Shen D. Wang, E. Langlois, W.A. Barrow, P.J. Green, C.W. Tang, J. Shi, *Degradation mechanisms in organic light emitting diodes*, Synthetic Metals 111112 (2000) 233-236.

[38] S. Karg, J. Steiger, H. von Seggern, *Determination of trap energies in Alq_3 and TPD*, Synthetic Metals 111-112 (2000) 277-280.

[39] J. McElvan, H. Antoniadis, M. R. Hueschen, J. N. Miller, D. M. Roitman, J. R. Sgeats, R. L. Moon, *Formation and growth of black spots in organic light-emitting diodes* Journal of Applied Physics 80 (1996) 6002-6007

[40] S. F. Lim, W. Wang, S. J. Chua, *Degradation of organic light-emitting devices due to formation and growth of dark spots*

[41] M. Ishii, Y. Taga, *Influence of temperature and drive current on degradation mechanism in organic light-emitting diodes* Applied Physics Letters 80 (2002) 3430-3432

[42] G. Baldacchini, T. Baldacchini, A. Pace, R. B. Pode, *Emission Intensity and Degradation Pocesses of Alq3 Films* Electrical and Solid State Letters 8 (2005) J24-J26

[43] M. A. Lampert, P. Mark *Current Injection in Solids*, Academic Press, Inc.,New York, NY, 1970.

[44] S. Berleb, W. Brẗting, M Schwoerer, *Anomalous current-voltage characteristics in organic light-emitting devices*